Electric impedance spectroscopy on polymer light-emitting diodes a qualitative approach

Kilic, M.

Award date:
2004

Electric Impedance Spectroscopy on polymer light-emitting diodes: a qualitative approach.

Murat Kilic

February 2004

Study performed at Philips Research Eindhoven (Nat.Lab.) in cooperation with Eindhoven University of Technology (TU/e).

Group Polymer Physics (PFY)
Department of Applied Physics, Eindhoven University of Technology

Supervisors: Dr. P. A. Bobbert (Eindhoven University of Technology)
Dr. A. van Dijken (Philips Research, Nat.Lab.)

Abstract

The aim of this study was to use electrical impedance spectroscopy as a tool for deriving an electronic device model for polymer light-emitting diodes (PLEDs). By modeling the organic layers present in PLEDs as parallel RC elements, the capacitive behavior of these devices at low modulation frequencies shows an interesting voltage-dependency that can be subdivided into three different regions:

1. At applied voltages below the built-in voltage of the device, a voltage-independent capacitance is observed, the value of which depends on the presence of a PEDOT:PSS layer, and additionally on the resistivity of this layer.
2. Close to the built-in voltage of the device, a capacitance maximum is observed which can be ascribed to trapping (and detrapping) of charge carriers at the interface between the PEDOT:PSS layer and the light-emitting polymer layer. The occurrence of this feature depends strongly on the type of light-emitting polymer used.
3. At applied voltages above the built-in voltage of the device, a gradual increase of the capacitance is observed, due to the space-charge limited nature of charge transport through the device.

Contents

1 Introduction

At Philips research laboratories there is a growing need to have a model that describes the physical behavior of a polymer light-emitting diode (PolyLED). Although there exists some models for PolyLED devices, which consist of Au/OC_1C_{10}-PPV/Cu [1] or ITO/PPV/Ca [2], these are outdated because the current day PolyLEDs have an extra planarizing layer of highly-conductive poly(ethylenedioxidethiophene)-poly(styrene sulfonic acid) (PEDOT:PSS). The aim of this research is to characterize the physical behavior of these new PolyLEDs by means of electrical impedance spectroscopy and *J-V* measurements and hereby extracting determining the key parameters that influence the device behavior.

1.1 Historical background

Nowadays, polymers are widely used in the industry because of their high strength, light weight, ease of chemical and physical modification, and processability at low temperatures. However, the usage is limited to insulating polymers as substitutes for materials like metal and wood [2]. In the 1950s and early 1960s the first steps were taken towards electrically conducting polymers by studying organic anthracene molecules in the crystalline state [3-5]. These molecular crystals exhibited semiconducting properties such as photoconductivity [6, 7] and electroluminescence [3], but still they were considered as exotic materials with little possible applications due to their poor performance [8, 9]. Halfway 1960s molecularly doped polymers, which are formed by dispersing chromophores (organic pigment) in an insulating polymer matrix, appeared and were intensively investigated thereafter [10-12]. Shortly hereafter, chromophores were built into the polymer as side groups or even in the main chain of the polymer itself so as to synthesize semiconducting polymers. In 1977 the discovery of a highly conductive organic polymer, chemically doped polyacetylene, demonstrated the active involvement of the polymer in the conduction of electrical charge [13]. Hence, the range of electric conductivities now accessible covers values typical for insulators (~ 10^{-10} S/cm), semiconductors (~ 10^{-5} S/cm) and metals (~ 10^{5} S/cm for copper) [14]. At the end of the 1980s the interest in undoped organic semiconductors, i.e. polymers as well as small molecules, revived with the demonstration of high-performance electroluminescent devices, which consist of multilayers of vacuum-sublimed dye films, made at Eastman Kodak [15], the report of FETs made from polythiophene [16, 17] and from small conjugated oligomers [18, 19], and the discovery of electroluminescence from conjugated polymer-based diodes at Cambridge University [20]. At the moment the most promising of these two organic semiconductors are conjugated

polymers because they have an intrinsic advantage over the small organic molecules due to their better mechanical properties and processability. Hence, a lot of research is focused on conjugated polymers at various laboratories across the world of companies such as Philips, Cambridge Display Technologies, Seiko Epson, etc.

1.2 Conjugated Polymers

Conjugated polymers are polymers that have a one-dimensional path of alternating short and long carbon-carbon bonds along the backbone of the polymer chain even for ring-containing polymers like poly(*p*-phenylenevinylene) [21]. These alternating short and long bonds are single C-C bonds as in ethane with a bond length of 1.54 Å and double C-C bonds as in ethylene with a bond length of 1.33 Å [22]. According to the Molecular Orbital Theory the 2*s* orbital of C has been hybridized with two of the three available 2*p* orbitals to form three hybrid orbitals: sp^2 hybrids. These three orbitals lie in a plane at certain angles to each other. The third unhybridized 2*p* orbital is oriented perpendicular to the sp^2 plane and is usually called p_z orbital. So, when two sp^2-hybridized carbons approach each other, they form a strong σ-bond by sp^2-sp^2 overlap. At the same time the unhybridized p_z orbitals on each carbon approach each other to form a π-bond provided that they have the correct geometry for sideways overlap. This has been illustrated below in the case of polyacetylene [1].

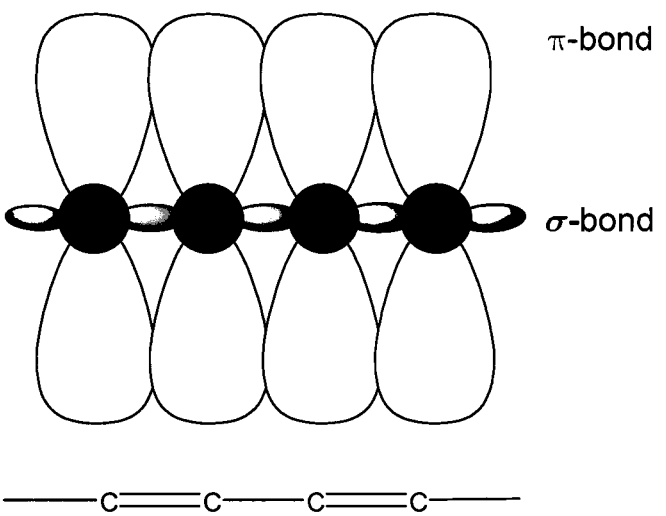

Figure 1.1 A schematic representation of bonding in polyacetylene. The black spheres represent carbon atoms. Hydrogen atoms and corresponding bonds are not shown for clarity reasons.

The electrons residing in the σ-bonds are highly localized whereas π-electrons are delocalized within a molecule due to the orbital overlap. Hence, the energy gap between the highest occupied molecular orbital (HOMO) and the lowest unoccupied molecular orbital

(LUMO) is relatively small, i.e. with transition frequencies within the visible range [2]. Most conjugated polymers have band gaps between 1.5 and 3.0 eV.

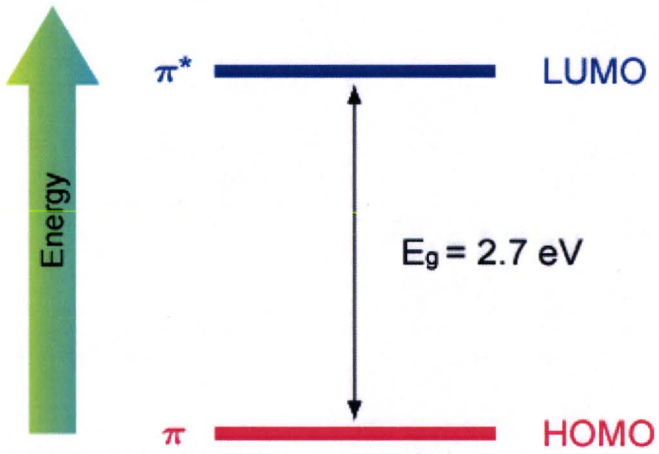

Figure 1.2 An energy-level diagram for poly(*p*-phenylenevinylene). An electron promoting from a bonding (π) molecular orbital to an antibonding (π*) orbital is called a π → π* excitation.

The extended π-bands account for the alluring electrical and optical properties of conjugated polymers. Conjugated polymers are intrinsically semiconducting due to the absence of partially filled bands. So, when charge carriers (electrons or holes) are added the polymer becomes conductive. The carriers that are injected or created (by means of chemical doping) in a conjugated polymer traverse along the polymer backbone via the π-bands, thus creating high conductivity. Additionally, the carriers can also hop from one molecule to another provided that the polymer molecules are close to each other. In general, the polymer chains lie tangled up and an increase of the material order can reduce the distance between the polymer molecules and thereby improve carrier mobility viz. charge hopping. However, chemical defects (cross-links, impurities, etc.) and physical defects (kinks, twists, etc.) can disrupt the π-conjugation beyond a certain distance, which is called the conjugation length, and suppress the one-dimensional nature [1]. Furthermore, structural disorder plays an important role over lengthscales longer than 10 nm. These two effects combined influence the interaction and charge transfer between weakly (Van der Waals) coupled conjugated polymer chains, because these defects introduce spatially localized states in the forbidden energy gap that can trap mobile carriers, so that they can no longer contribute to the conductivity until they are released again. As it will be shown in the results, this relaxation process can be accelerated by means of photo-absorption and/or thermal-activation.

The most popular and studied conjugated polymer is poly(*p*-phenylenevinylene) (PPV), of which the chemical structure is depicted in Figure 1.3. Spectroscopic studies [23] in conjunction with theoretical modeling [24, 25] indicate that the effective chromophore in PPV extends over 7-15 repeat units, with conformational and chemical defects preventing extended conjugation over the entire chain, hence the emission maxima of PPV are around 2.25 and 2.4 eV, i.e. the yellow-green region of the visible spectrum. PPV is insoluble,

intractable and infusible; consequently PPV derivatives with solubilizing side chains could be used as precursor to make this polymer soluble [26] in order to easily process it with the spin-coating technique.

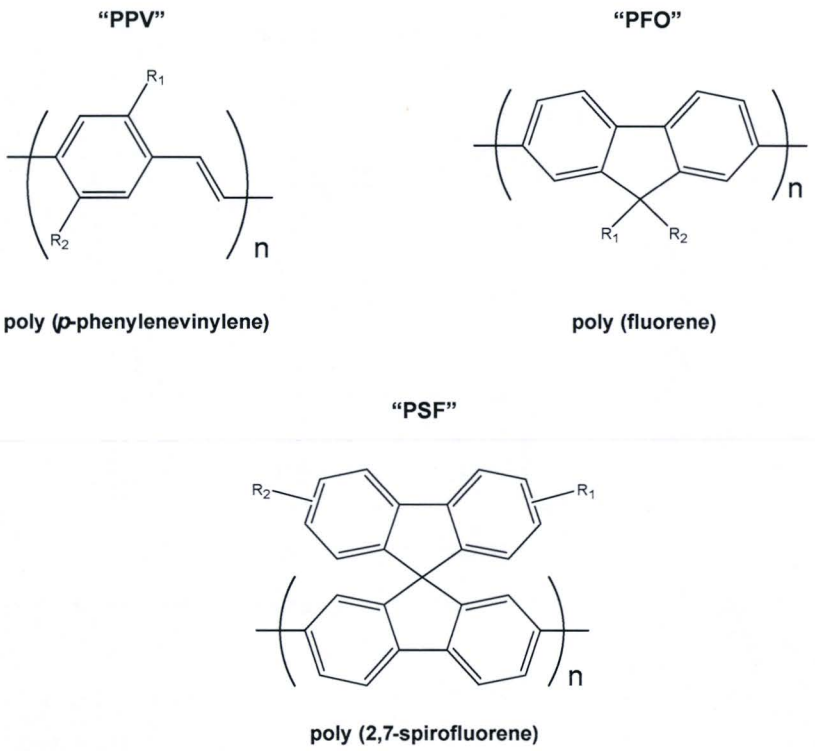

Figure 1.3 Chemical structure of the most common conjugated polymers used within the framework of this research at Nat.Lab. (Philips Research Laboratories). Hydrogen atoms are not shown for clarity reasons.

Another important family of conjugated polymers that covers the blue-emitting region is poly(*p*-fluorene) (PPP). A well-known branch of this family is poly(fluorene) (PFO), which has a planar structure, as can be seen in Figure 1.3, due to the extra-bridge between the two phenyl-rings in a mer-unit. However, the conjugation length is still relatively short and hence it emits light in the blue region. It is desired to increase the efficiency of emission in the blue-region and also to prevent poly(fluorene) of forming nicely ordered stacks, which could increase the conjugation length. Therefore poly(2,7-spirofluorene) (PSF) is used instead. This polymer has a non-planar staggered structure, of which the mer-unit is built up out of two fluorene groups, as depicted in Figure 1.3. The properties of these PPP-derivatives depend highly on the way the conjugated polymer is synthesized. Different methods such as a combination of precursor polymer and phosphoric acid-catalyzed process [27] or the Kovacic process [28] can be used to synthesize PPP polymers [26]. Nowadays, PPP-derivatives with solubilizing side-chains are the most important [29].

In research that was conducted within the framework of this report mainly PPV-, PFO- and PSF-derivatives with different classified side-groups have been used. More details on these polymers will follow in the subsequent sections based on necessity due to the confidential nature of these materials.

1.3 Applications

Since the discovery of electrically conducting polymers they have steadily replaced other conducting materials in various applications or they have opened ways to novel applications. In electrophotographic devices like photocopiers and printers multilayers of organic photoconductors (semiconducting polymers) have steadily replaced the amorphous-selenium (a-Se) and amorphous-silicon (a-Si) photoreceptors [30]. Conversely, highly conducting polymers, of which chemically doped polyacetylene was one of the first, are used as coatings for electrostatic dissipation and electromagnetic shielding [31]. Applications of undoped organic semiconductors, both polymers and small molecules, have begun to emerge in photovoltaic devices such as solar cells [32], in integrated circuits (ICs), which are arrays of transistors. Remark that, it is unlikely that these materials will be used in central processing units (CPUs) due to the fact that the clock frequency of an electronic device is proportional to the charge-carrier mobility, which is smaller for organic semiconductors than for single-crystalline silicon (c-Si). However, low-speed (up to 10^3 Hz) applications in recyclable electronics such as product tagging or identification could be achieved.

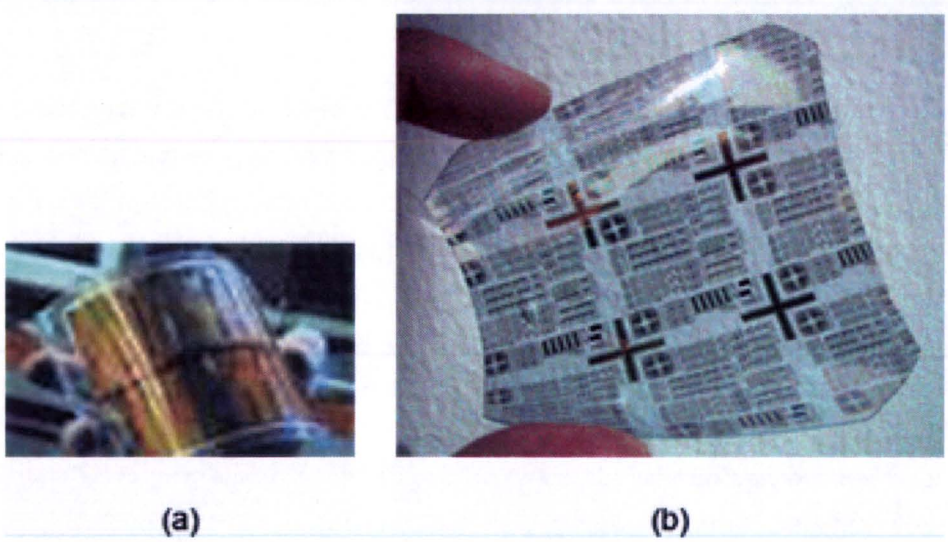

Figure 1.4 (a) A photovoltaic device made of organic semiconductors (BioMaDe Technology 2003). (b) A RF ID tag made of polymer-based ICs (Infineon Technologies AG 2003).

Yet the most important branch of applications for organic semiconductors are flexible displays, i.e. full color matrix displays. Several Japanese companies have already started with active-matrix full color small molecule Organic Light Emitting Diode (OLED) displays. Up till now the largest one has been produced by Sony: a 24-inch display consisting of four integrated 12-inch individual small molecule OLED (smOLED) panels[†].

[†] Source: Philips IPO Japan

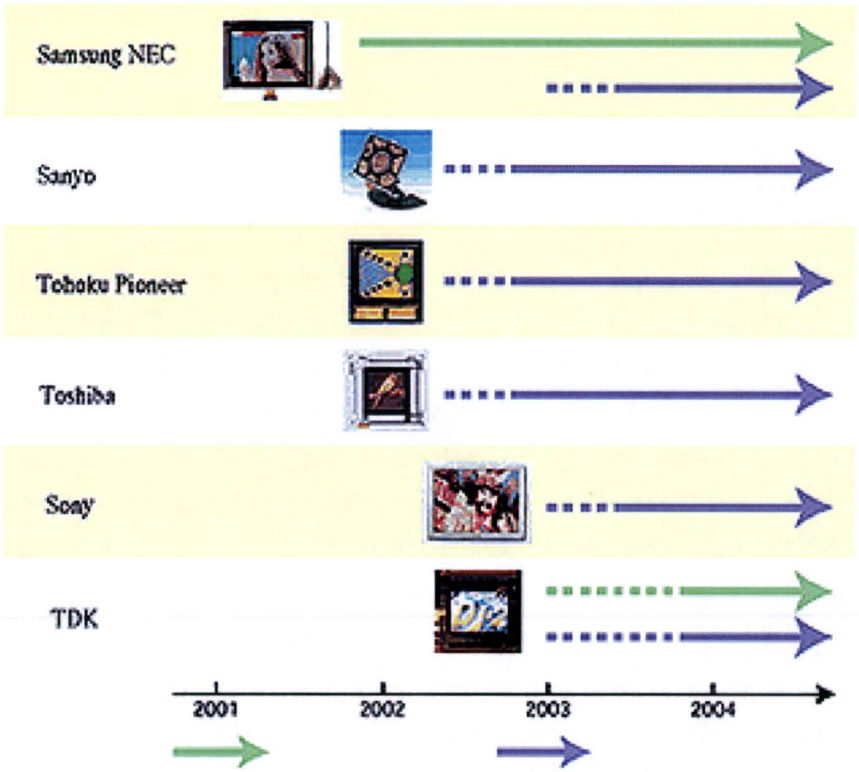

Figure 1.5 The progress of Japanese companies over the last few years in smOLED (purple arrow) and polymer OLED (green arrow).

As mentioned earlier conjugated polymer OLED (PLED or PolyLED) displays could be more flexible and cheaper to realize due to its ease of processability and mechanical properties. Philips has chosen this path for its OLED display technology and is concentrating its research efforts on PolyLED displays in order to achieve large-scale full-color matrix displays. The advantages that PolyLED displays would have over LCD-displays are:

- High brightness and contrast due to electroluminescent nature of the material and the lack of backlighting
- Large-angle viewing
- Low-voltage operation so less power-consumption
- Flexibility (foldable, bendable)
- Fast switching speeds
- Thin and lightweight

Philips has already fabricated some small-scale PolyLED displays such as the status indicator incorporated in the new men's shaver Sensotec, as can be seen in Figure 1.6. Also prototypes of full-color PolyLED matrix displays have been demonstrated by Philips, of which examples are shown in Figure 1.6.

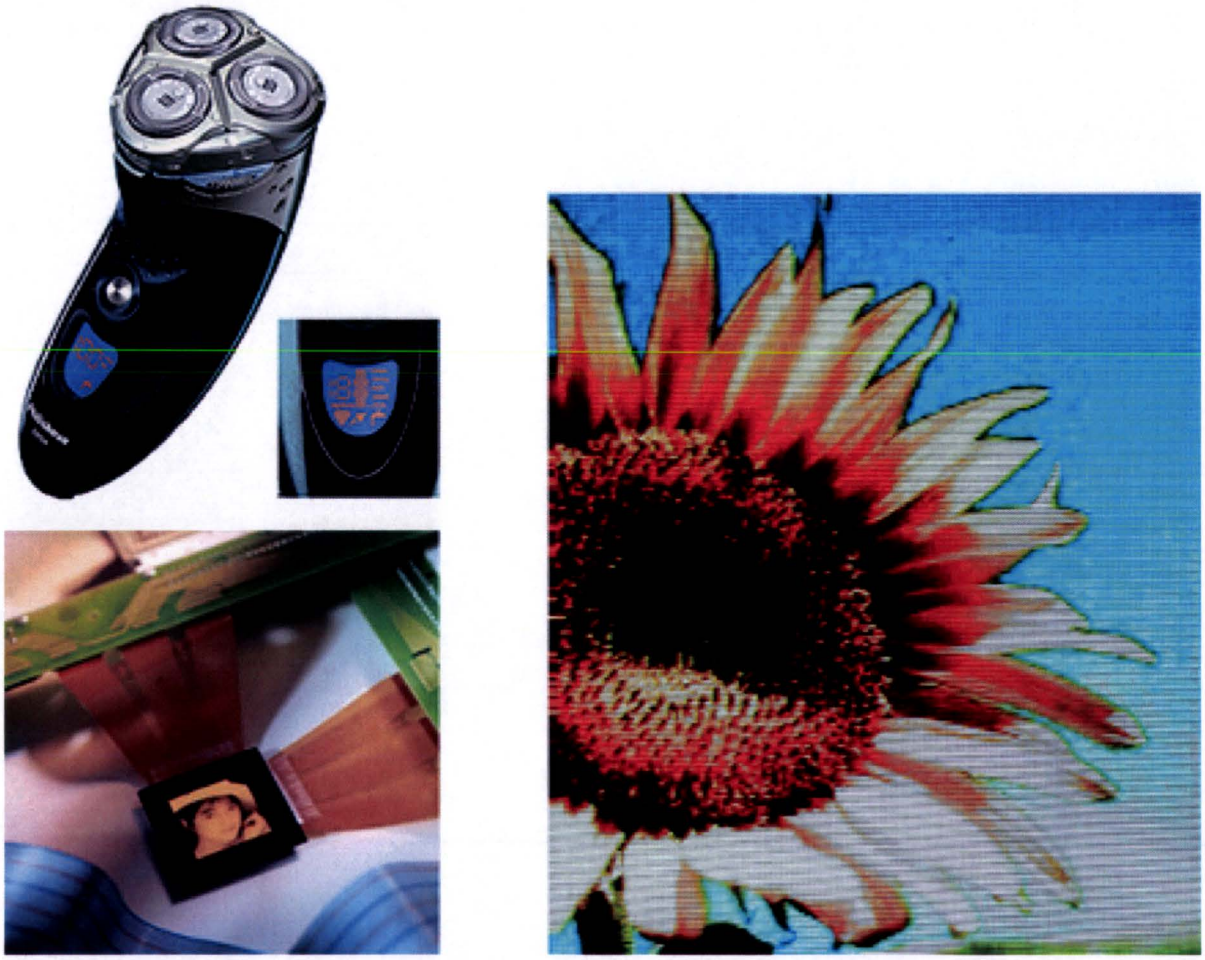

Figure 1.6 Upper left photo shows the Sensotec men's shaver with the status indicator (PolyLED display) enlarged next to it. Lower left photo shows a monochrome active-matrix PolyLED display. Right photo shows a full-color active-matrix PolyLED display. (Source photos: Philips).

The current focus at Philips Research is to increase the lifetime of the PolyLED displays especially by increasing the lifetime and efficiency of the blue-emitting conjugated polymer by means of, among other things, triplet emitters, to optimize the fabrication of large-scale displays at low costs via e.g. inkjet-printing, and to understand the device physics in order to built a solid model of how the device functions.

2 Polymer light-emitting diodes

In this chapter the functioning of polymer light-emitting diodes will be explained. Also the theoretical background will be treated in relation to the current state of affairs in literature.

2.1 What is a polymer light-emitting diode?

A typical polymer light-emitting diode consists of a thin layer (typically 80 nm) of unintentionally doped (pristine) light-emitting polymer on top of a hole transport layer (HTL, typically 100 – 200 nm) made of poly(3,4-ethylenedioxythiophene):poly(styrene sulfonic acid) (PEDOT:PSS, typically 1:6), a *p*-type conducting polymer. The HTL has a double function: (a) it facilitates the hole-injection from the anode, which is usually made of pre-cleaned Indium-Tin-Oxide (ITO) coated on glass substrates, and (b) it acts as a planarizing layer for the rough ITO surface thereby minimizing the occurrence of short-circuits due to direct contact between ITO and the cathode. On top of the light-emitting polymer (LEP) layer a metal cathode is evaporated. The metal used has a low work function, as it should inject electrons into the LEP layer under forward bias of the device. A metal that can be used for this purpose is Ba. A typical cathode consists of a 5 nm Ba layer, capped with a 100 nm Al layer. The Al layer serves to protect the Ba layer from oxidation and to lower the contact resistance.

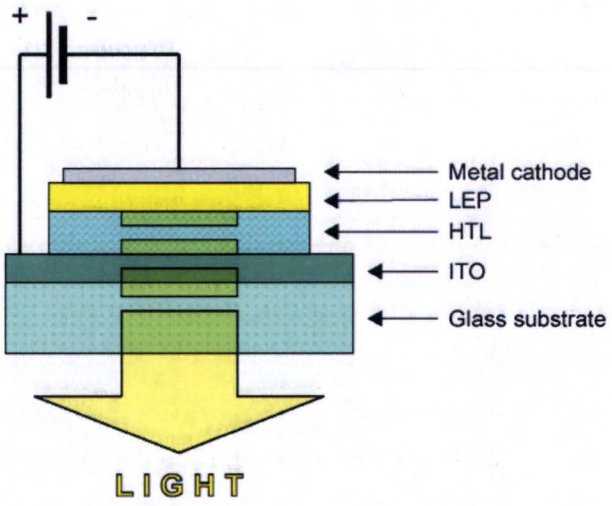

Figure 2.1 A schematic diagram of a typical polymer light-emitting diode.

Under forward bias electrons are injected from the cathode and holes from the anode. The charge carriers, driven by the applied electric field, move through the polymer over a certain

distance until recombination takes place. Hence, light is generated via electroluminescence (EL). Thus, the device operation of a polymer light-emitting diode is determined by: charge-injection, charge-transport, and recombination [33]. For the understanding and optimization of polymer light-emitting diodes it is important to develop a description of the device characteristics. For instance, it has already been demonstrated by Blom et al. [2] that for poly(*p*-phenylenevinylene) (PPV) as LEP the current is mainly carried by holes, whereas the light-output is governed by the presence of both electrons and holes.

In the following paragraphs a more detailed overview of theoretical principles concerning polymer light-emitting diodes will be given to explain and illustrate the functioning of such devices.

2.2 Solid-state physics

The forming of σ-bonds and π-bonds via sp^2-hybridization was already briefly treated for polyacetylene. Now let us look at the formation of these bonds a little closer by examining the archetypal building block of a conjugated polymer: ethylene. The electronic configuration of hydrogen is $1s^1$ and that of the ground state of carbon is $1s^2 2s^2 2p^2$. So, carbon has four electrons in the outer shell (n=2), two of which are paired in the 2*s* orbital (l=0), and two of which are unpaired in different 2*p* orbitals (l=1, m_l = -1, 0, 1). The molecular orbitals (MO's) can be formed from a linear combination of these atomic orbitals (AO's) via the LCAO-method [34]. The ground-state properties of this molecule can be calculated by means of the Hartree-Fock theory. However, for extended systems the electron-electron correlation effect has to be taken into account, which can be done by using the Möller-Plesset perturbation theory (MP*n*, with *n* the order of the perturbation theory) [35] or the Configuration Interaction (CI) theory [36] instead of the Hartree-Fock theory. Instead of presenting a thorough mathematical argumentation of the MO's in this report, a qualitative approach will be used. So, the MO's are filled bottom-up with the available electrons. The filled orbitals (binding MO's) and the unfilled orbitals (antibonding MO's, indicated by an asterisk), created from the AO's are depicted below.

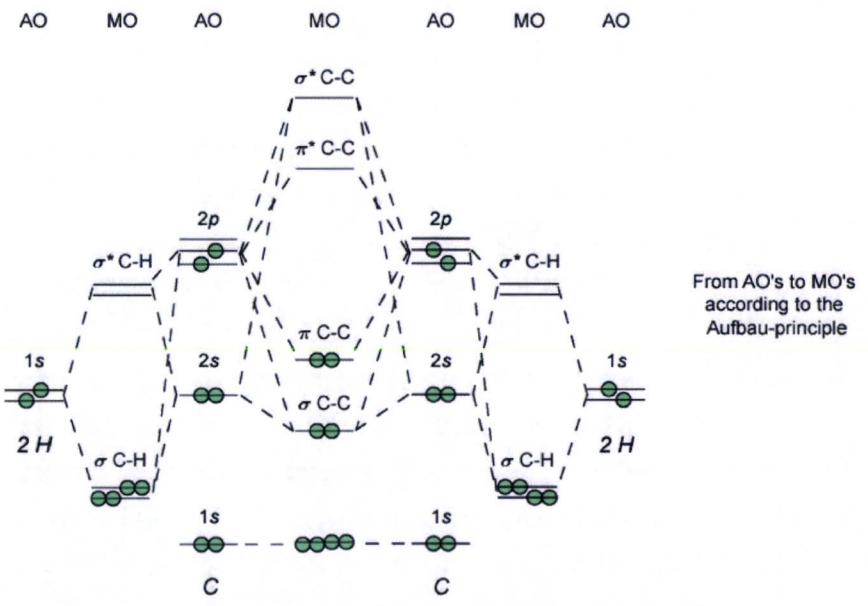

Figure 2.2 A schematic diagram of how the molecular orbitals (MO) of ethylene are constructed from the atomic orbitals (AO) of hydrogen (H) and carbon (C) according to the Aufbau-principle.

As deeper lying MO's do not play an important role for the optical and electrical properties, a simplified notation for the electronic configuration of ethylene in the ground state is π^2, indicating that the highest occupied molecular orbital (HOMO) has π character and contains two electrons. The lowest excited state of the ethylene molecule is attained when one electron is excited into the lowest unoccupied molecular orbital (LUMO) by means of a $\pi \rightarrow \pi^*$ transition, as depicted in Figure 1.2. The electronic configuration of this excited state is denoted as (π, π^*). The strength of the double bond is lower in the excited state than in the ground state, because the MO of the excited state (π^*) is antibonding of character. Higher-energy excitations such as $\pi \rightarrow \sigma^*$ and $\sigma \rightarrow \pi^*$ are not relevant for the device operation of polymer light-emitting diodes, and are consequently not discussed here.

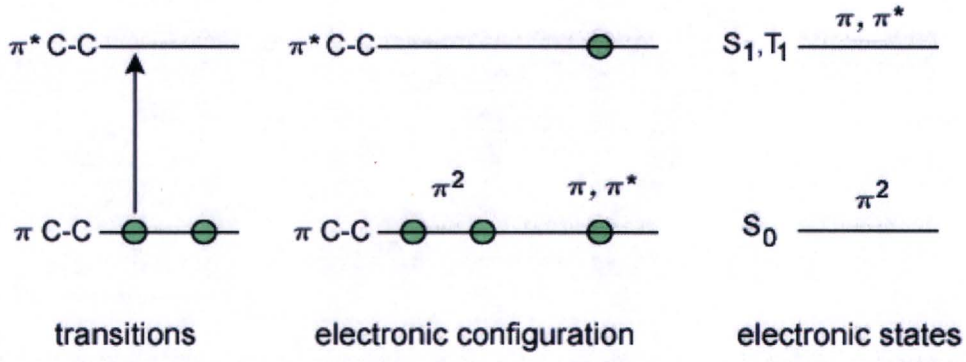

Figure 2.3 The $\pi \rightarrow \pi^*$ transition is a promotion of an electron from the ground state S_0 with electronic configuration π^2 to an excited state S_1 or T_1 with electronic configuration (π, π^*).

According to the Pauli principle the ground state configuration must be a singlet state S_0 (S=0), meaning that the spins of the two electrons in each MO are paired, i.e. they have opposite sign and the net spin moment is zero. However, in the excited state an electron has been promoted to a different MO and thus there are two distinct MO's (π and π^*) that contain one electron and the Pauli principle does not require these electrons to be paired. Hence, there exist two excited states with the same electronic configuration, but with different net spin momenta: (a) a singlet excited state S_1 (S=0) in which both spins are anti-parallel and (b) a triplet excited state T_1 (S=1) in which both spins are parallel. Quantum mechanics dictates that the triplet state is triply degenerate, i.e. there are three triplet levels with different orientation of net spin (M_S=+1, 0, 1) with respect to a certain molecular axis. The energy of a triplet state is lower than the energy of a singlet state of the same electronic configuration: $E(S_1) > E(T_1)$ [34]. The energy difference, which is responsible for the S-T splitting, is a result of the exchange interaction. Calculations show that this interaction is only present for singlet states, hence increasing its energy [21].

The polymers that are used in polymer light-emitting diodes are usually conjugated polymers, which mean that they contain alternating single and double bonds, and consequently show π-delocalization: the bonding (and anti-bonding) valence electrons are "smeared" out over many bonds due to the fact that the AO's of many carbon atoms take part in the formation of the HOMO and LUMO. Adding more and more interacting orbitals will result in a completely filled valence band, which is the range of energies covered by the orbitals, and a completely empty conduction band. So, adding orbitals fills the energy range to form energy bands and concomitantly lowers the energy separation between the HOMO and LUMO.

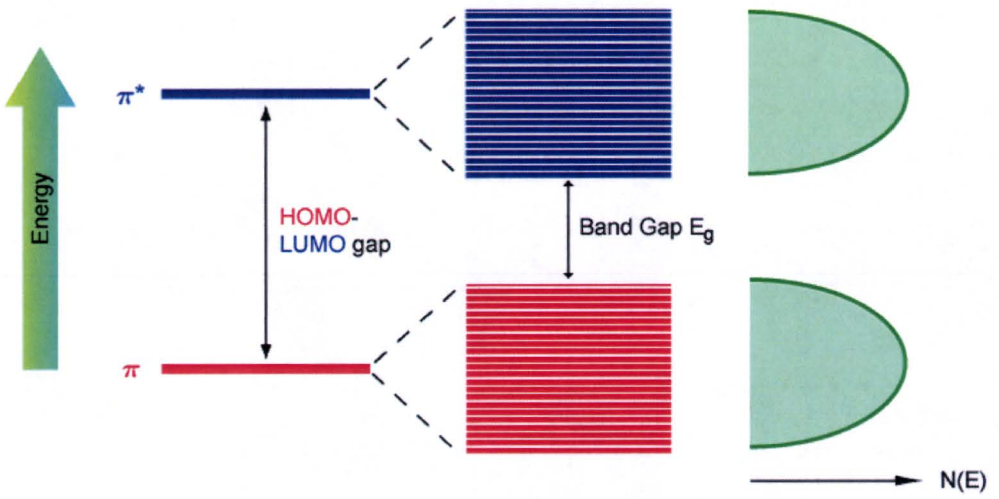

Figure 2.4 The band energy diagram is shown for the case that the HOMO and LUMO levels devolve to energy bands by many interacting AO's from the polymer chain. On the right side, the density of states $N(E)$ as a function of energy is shown.

The density of states N, depicted in Figure 2.4, is typical for polymers. In molecular crystals, in which all conjugated bonds are aligned perfectly, one would expect a different density of states (DOS), i.e. $N(E) \sim 1/\sqrt{E}$, due to Van Hove singularities [37]. Additionally, polymers such as used in polymer light-emitting diodes contain many chemical and structural defects and are amorphous, i.e. there is no extended regular stacking of monomers in any direction. Consequently, there is a random distribution of conjugated segments of various lengths in a polymer chain, which are dependent on subtle interactions with other polymer chains. This random morphology introduces structural and energetic disorder, hence resulting in a Gaussian DOS, which is lowest at the edges of the energy bands.

When an electron is excited to the conduction band, a hole is left in the valence band. Following this excitation, the electron relaxes to the bottom of the conduction band, while the hole relaxes to the top of the valence band.

When an electric field is applied, the electrons and holes will be transported in opposite direction through the conjugated π-system. In a polymer light-emitting diode the injected charge carriers are transported in opposite direction through the conjugated π-system, until they come so close together that they "feel" the mutual Coulomb interaction. This attractive force implies a lowering of the energy if they stay together. Such an electron-hole pair is called an exciton. It is important to realize that an exciton is essentially a (π, π*) electronic state which is mobile, and which is electrically neutral. The formation of both singlet and triplet excitons through "binding" of free electrons and holes is at the heart of the operating principle of polymer light-emitting diodes. The probability of a singlet exciton to appear by recombination of an electron and a hole can be deduced by spin statistic arguments [38]: since two electron spins can recombine in one singlet state or three triplet states, the probability P that a singlet state will be generated is

$$P = \frac{1}{1+3} \cdot 100\% = 25\% \qquad (2.1)$$

The argument above holds only if there is an equal probability in generating a singlet or triplet state. But then again, it has been reported that some polymers offer up to 75 % singlet yield [39, 40]. A satisfactory answer for this result has still to be provided.

Dissociation of the exciton does not readily occur, because the exciton binding energy (ΔE^b), which is typically 0.4 eV (see Figure 2.5), is considerably higher than the thermal energy at room temperature (0.026 eV).

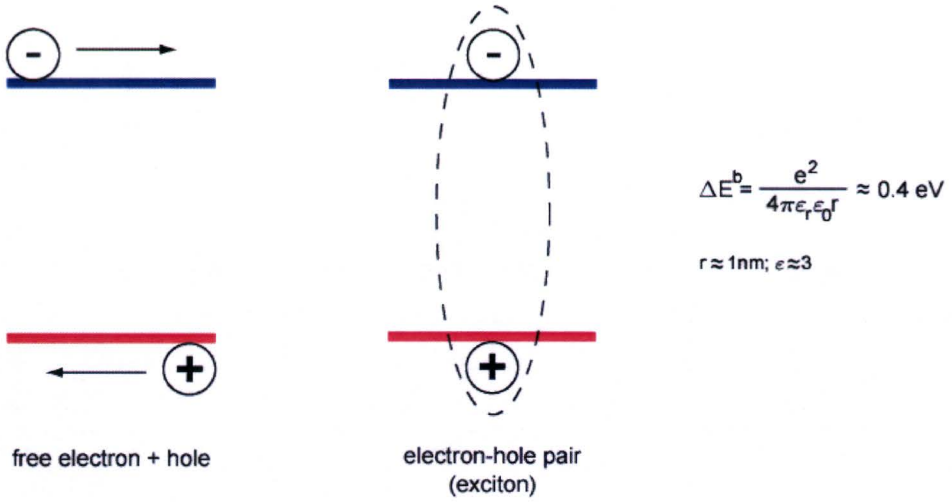

Figure 2.5 A Frenkel-exciton, which is a strongly bound exciton, is created via Coulomb-coupling of a free electron and hole upon releasing the exciton binding energy ΔE^b.

Excitons can be divided into two groups: Frenkel-excitons and Mott-Wannier excitons. A Frenkel-exciton is highly localized on a molecule and is able to hop from one molecule to another. Conversely, Mott-Wannier excitons are weakly bound and the average distance between the electron and hole is much greater than the nearest intermolecular distance [41]. The excitons observed in polymer-light-emitting diodes are of the type of Frenkel [42].

Usually the energy levels are compared on an absolute scale with as reference point the energy of an electron in vacuum. Then the relative position of the HOMO with respect to the vacuum is equal to the ionization potential (IP), which is the minimum energy required to remove an electron from the system. The relative position of the LUMO with respect to the vacuum is the electron affinity (EA), which is the maximum energy gained by adding an electron to the system.

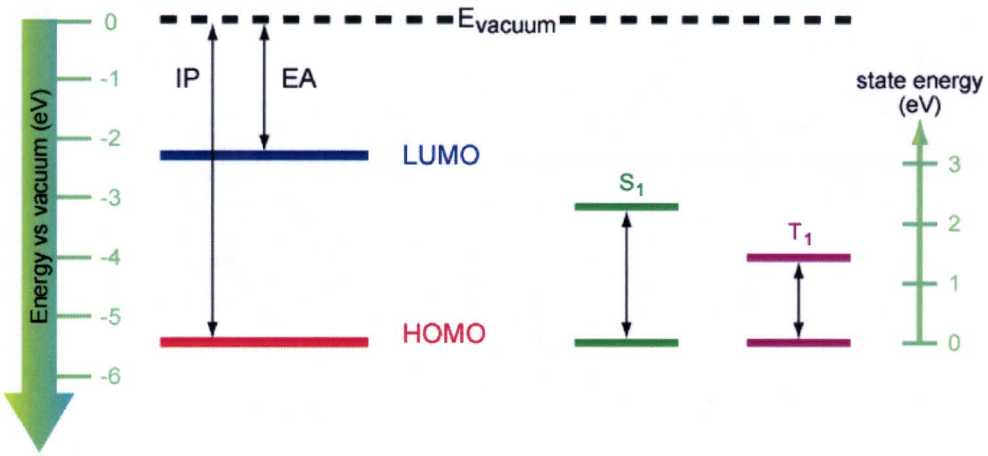

Figure 2.6 The energy levels of the LUMO and HOMO together with the singlet and triplet energy levels are depicted relative to the vacuum energy level. The values are for a typical PPV-derivative polymer.

The energy levels in Figure 2.6 of singlet and triplet states have been determined experimentally. Note that IP-EA is larger than the singlet exciton energy S_1. The difference is the exciton binding energy:

$$E_{IP} - E_{EA} = E_{LUMO} - E_{HOMO} = S_1 + \Delta E^b \tag{2.2}$$

The energy levels depend to some degree also on the nature of the side groups of a conjugated polymer. So, in this way the color of the luminescence can be tuned. In the next paragraph luminescence, which is a key process in polymer light-emitting diodes, will be explained further in detail.

2.3 Luminescence

Luminescence is the emission of all ultraviolet (UV), visible (VIS), or infrared (IR) electromagnetic radiation by atoms or molecules. The light wave is generated by the acceleration of electrical charges produced following the excitation of the luminescent center. The type of luminescence observed depends on the origin of excitation. Excitation of a LEP with photons leads to photoluminescence (PL), which is itself subdivided into fluorescence and phosphorescence according to the intermediate steps followed by the de-excitation process. Fluorescence is the emission of light from singlet excited states, i.e. $S_1 \rightarrow S_0$ emission, whereas phosphorescence is the emission of light from triplet excited states, i.e. $T_1 \rightarrow S_0$ emission. However, the key process in polymer light-emitting diodes is another type of luminescence: electroluminescence (EL). This is light emission under the action of an electrical current or field, in which the light generation and electrical power dissipation take place in one and the same nonincandescent material, such as a LEP. In polymer light-emitting diodes the current consists of holes injected from the anode and electrons injected from the cathode. These charge carriers can recombine into a singlet or triplet exciton depending on their mutual spin momenta, after which the system can return to its ground state by fluorescent or phosphorescent photon emission, respectively.

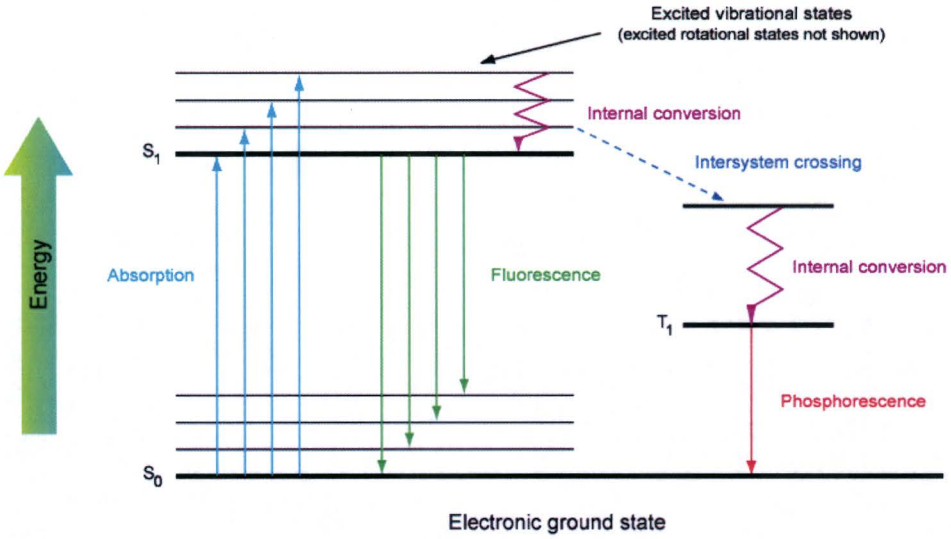

Figure 2.7 The processes occurring between the absorption and emission of light is illustrated in a Jablonski diagram.

Photon absorption brings the system usually not only in an electronically excited state, but also in a higher vibrational level. Internal relaxation to the ground state vibrational level takes place, while the system is still in the electronically excited state. This occurs typically on a ps time scale. The system is then in thermal equilibrium with its surroundings. Luminescence always takes place from systems in thermal equilibrium, since a (typical) decay time or lifetime of the excited state in LEPs ranges from 0.1 ns to several μs.

Luminescence can take place from the lowest vibrational level in the excited state to higher vibrational levels in the ground state. The combined effect of the vibrational relaxation in the ground and excited states is that the energy of emission is typically smaller than the energy required for excitation. This phenomenon is called Stokes shift after its discoverer. Exciton diffusion also leads to an energy difference between emission and excitation, due to the amorphous nature of the LEP. The variations in conjugation length and chemical surroundings induce a spread in the electron and hole energy levels. Hence, the exciton energy depends also on the location in the LEP: the exciton has relatively high energy for short conjugation length (large HOMO-LUMO gap) and relatively low energy for large conjugation length (small HOMO-LUMO gap). The exciton strives to lower its energy during its lifetime of 1 ns, in which it can travel up to 10-20 nm. Thus, high-energy excitons, which are created by absorption, will emit light as low-energy excitons. This leads to an increased Stokes shift, but also contributes to a broadening of the emission band and the occurrence of a "red tail" in the emission, characteristic of some segments in the LEP of exceptionally large conjugation length.

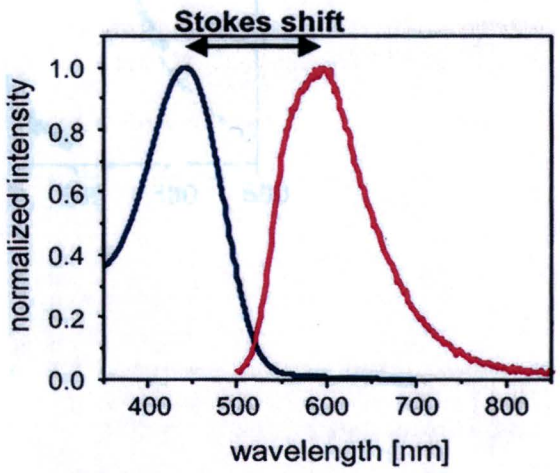

Figure 2.8 Stoke shift observed in a typical PPV-derivative LEP.

There are several other processes that can lead to an energy difference between emission and excitation such as intersystem crossing (ISC), which is a spontaneous conversion of a singlet excited state (S_1) into a triplet excited state (T_1), complex formation in the excited state (excimer or exciplex), and energy transfer. These processes also induce a depopulation of S_1 and consequently decrease the fluorescence intensity. The latter process, i.e. energy transfer, is transfer of excited state energy from an initially excited donor D (polymer) to an acceptor A (dye or defect). The donor emits at shorter wavelength (higher energy) than the acceptor. Thus, energy transfer is a downhill process in terms of energy and leads to a energy difference between emission and excitation. Efficient energy transfer can only occur when the emission spectrum of the donor and the absorption spectrum of the acceptor overlap (resonance). Sometimes LEPs are doped with a dye - typical concentrations are between 1 and 5 % - so that after excitation of the LEP all the excitons are funneled to the sites with the lowest excited state energy, in this case the dye. Energy transfer and doping are very important to the development of LEPs: imagine one can obtain green and red emission by doping a good blue-emitting material with suitable dyes, while maintaining the other good properties of the host such as stability and conductivity.

The efficiency of light emission by LEPs can be quantified by using a parameter called quantum yield or quantum efficiency (*QE*), which is defined as the ratio of the number of photons emitted with respect to the number of excited states initially present.

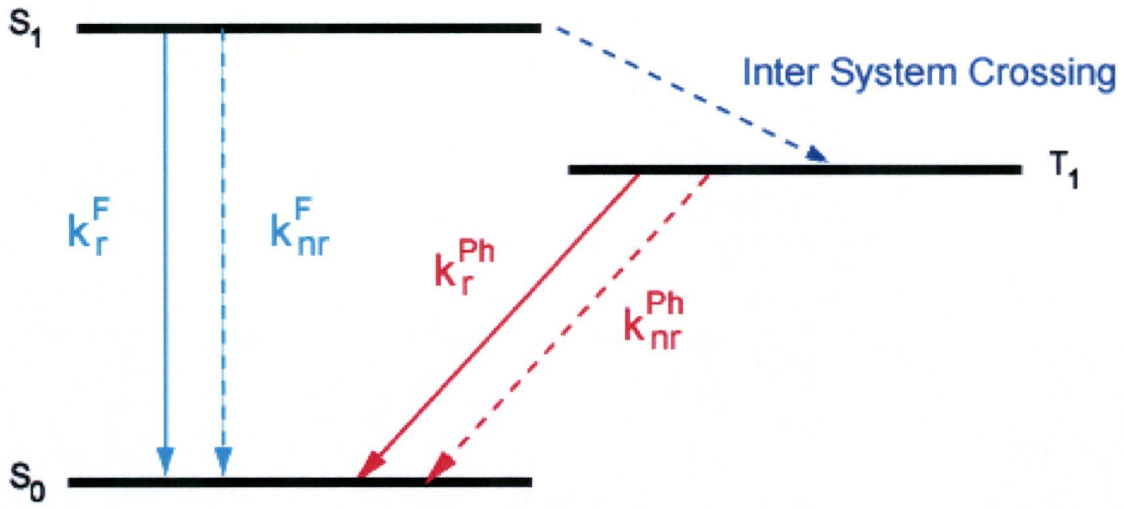

Figure 2.9 Schematic representation of different processes occurring after an excitation with decay rates *k* for each process.

In Figure 2.9, the subscript *r* refers to a radiative process involving the emission of photons, while the subscript *nr* refers to a non-radiative process, where the energy is dissipated in the form of heat. The superscripts refer to fluorescent (F) processes or phosphorescent (Ph) processes. A radiative decay at room temperature from the triplet excited state to the singlet ground state is unlikely to occur (i.e. $k_{nr}^{Ph} < k_r^{Ph}$) due to the spin forbidden nature ($\Delta s \neq 0$) of this optical transition. A radiative decay from the singlet excited state to the singlet ground state will be more likely, because this optical transition is spin allowed ($\Delta s = 0$). The quantum yield for the radiative recombination of singlet excitons is given by

$$QE^F = \frac{k_r^F}{k_r^F + k_{nr}^F} \tag{2.3}$$

Singlet excitons in good LEPs show quantum yield values above 15 %, even up to 100 % if dye-doped systems are used [43]. Triplet excitons, on the other hand, have values 1000 times lower than singlet excitons. Thus, practically all triplet excitons formed in a π-conjugated LEP decay to the ground state via nonradiative processes, unless special dyes are used, so-called triplet dyes or triplet-emitters. The fact that *QE* is lower than 100 % can be viewed as luminescence quenching. Several processes can lead to quenching: defects, which are present in the LEP due to the polymerization reaction, impurities due to the LEP processing and device manufacture, etc. These processes enhance the nonradiative decay so much that it competes with radiative decay. Although, the chemical nature of many defects in LEPs is not known and therefore their influences on *QE*, there are some exceptions: Photo-oxidation and field-induced quenching.

Photo-oxidation is the process in which the energy of an exciton is used to excite molecular oxygen resulting in a scission of the polymer chain and creation of two carbonyl

(C=O) groups, when the LEP is measured in ambient conditions. These carbonyl groups dissociate excitons in the vicinity and hence are very efficient quenchers: a concentration of 0.5 % of carbonyl groups reduces the *QE* by 50 % [44].

Field-induced quenching is the process in which an applied electric field is stronger than the binding energy of the exciton, hence it is energetically favorable for an exciton to dissociate into a separate hole and electron with a negligible probability or recombining again, thus reducing the PL intensity.

Elimination of quenchers thus requires careful optimization of processing: purification, nitrogen atmosphere, exclusion of UV-light and compatibility of materials in a polymer light-emitting diode.

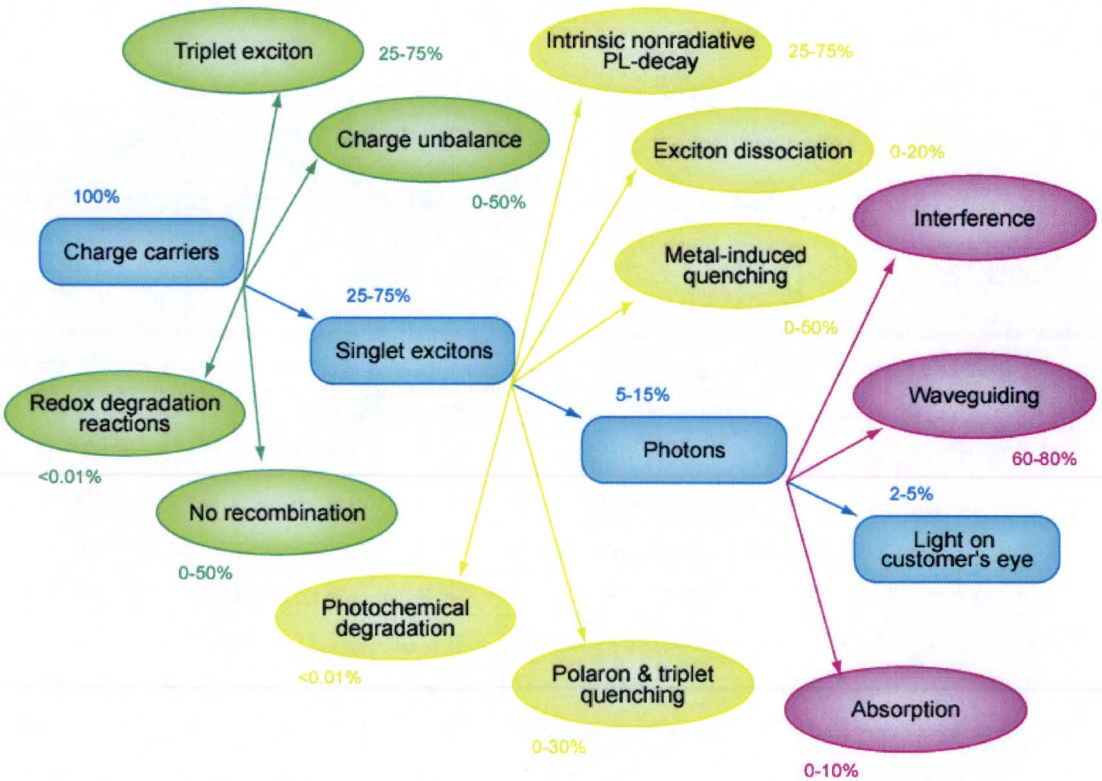

Figure 2.10 An overview of several loss mechanisms that determine PolyLED efficiency. The percentages are estimates for the contributions of all factors for current materials, i.e. host-dye systems with triplet emitters are not considered. The uncertainty is due to uncertainty for individual materials, variations between materials, and dependence on voltage. The box "photons" is the internal quantum efficiency; the box "light on customer's eye" is the external quantum efficiency. (Source: Philips Research).

In the next paragraph the electrical properties of the LEP and of the polymer light-emitting diode will be treated by looking at charge-injection, charge-transport and recombination.

2.4 *Electrical properties*

The understanding of charge-injection, charge-transport and recombination is very important in improving the performance of a polymer light-emitting diode. The diode performance depends on the nature of the active layer, the nature of the electrodes and their Fermi levels, and the diode structure. The active layer is characterized by a lot of dependent parameters such as relative position of energy levels, nature of the interface, size of the HOMO-LUMO energy gap, and the mobility of the charge carriers, influencing both charge-injection and charge transport.

Charge-injection, charge-transport and recombination will be presented one by one in the following sections.

2.4.1 Charge injection

In a polymer light-emitting diode holes are injected from the anode and electrons from the cathode. When no voltage is applied to the polymer light-emitting diode a reverse internal electric field is present in the diode prohibiting carrier injection from the electrodes. The internal electric field arises from the alignment of the Fermi levels of the anode, LEP and cathode at contact (according to thermodynamics) due to the asymmetric nature of the diode as a consequence of the use of dissimilar anode and cathode materials. At a certain positive applied voltage, which is called the built-in voltage V_{BI}, the internal electric field is zero. No current can flow as long as $V_{appl} < V_{BI}$. When the applied voltage is larger than V_{BI} injected holes and electrons experience a net electric field, which drives them to the opposite electrode allowing current to flow. An important consequence of the existence of V_{BI} is that a polymer light-emitting diode behaves like a diode.

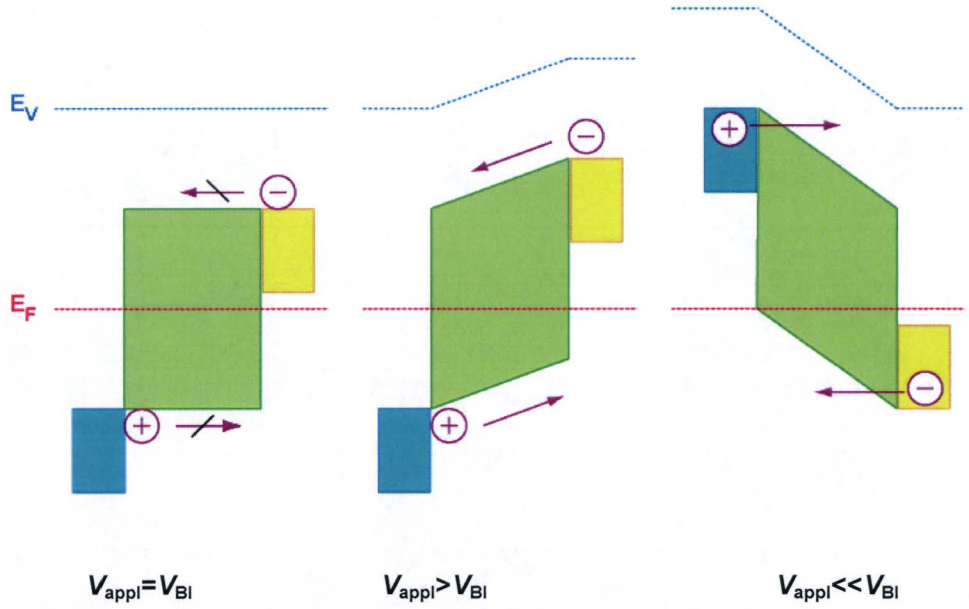

Figure 2.11 Influence of an external applied voltage on the relevant energy levels. $V_{appl}= V_{BI}$: the onset voltage for a device current at the flat band condition. $V_{appl} > V_{BI}$: injected electrons and holes can flow through the system as a result of the net electric field. $V_{appl} << V_{BI}$: current flow by tunneling effect.

The work function (Φ) of the anode needs to match the HOMO of the LEP to ensure efficient injection of holes. The requirements for electron-injection are *mutatis mutandi* the same as for holes. A good anode has a high work function such that holes do not experience an energy barrier at the interface. For instance, PEDOT:PSS has a high work function (5.0 eV) that matches the HOMO of a typical LEP such as PPV (5.2 eV) [45].

The nature of metal-polymer interfaces and their formation has been studied both experimentally and theoretically [46] and it has been demonstrated that hole transport in a typical LEP is bulk-limited and not injection-limited [47]. The charge carriers experience a small (negligible) energy barrier at the interface. Thus, injection of neither holes nor electrons is limiting and therefore the current is bulk-limited. So, an increase in current can be established by changing the electrical properties of the LEP.

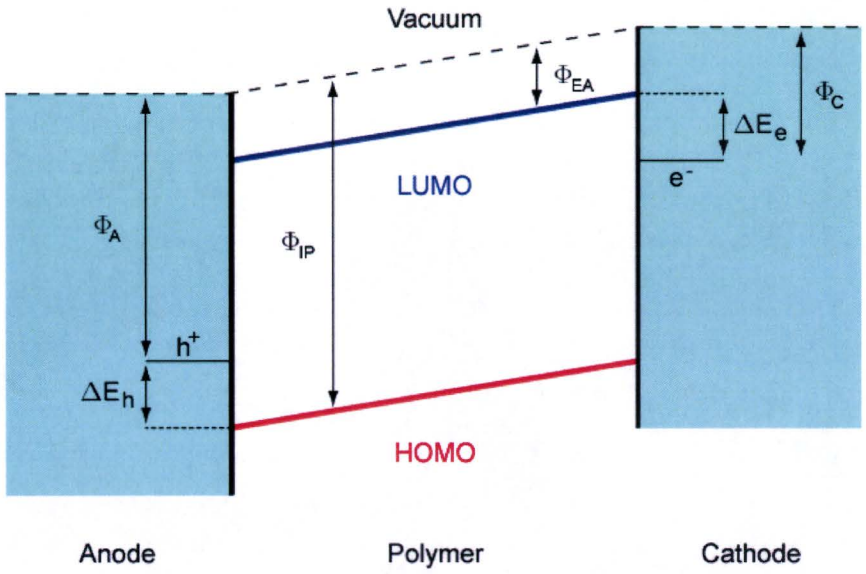

Figure 2.12 A schematic model describing the energy barriers ΔE_h and ΔE_e across which respectively the holes and electrons have to tunnel through [48, 49]. The work functions for the different energy levels are also shown.

In a first approximation one can say that $V_{BI}=(\Phi_A-\Phi_C)/q$. However, the formation of dipole layers due to charge transfer at the electrode polymer interface when $\Phi_C>\Phi_{EA}$ or when $\Phi_A<\Phi_{IP}$ leads to a decrease of the built-in voltage. In addition, chemical reactions at the interface can affect the work functions and thus alter V_{BI}. Therefore, optimization of anode and cathode injection has remained a rather empirical search.

It has been demonstrated by Blom et al. [2] that for hole-only devices space-charge limited (=bulk limited) current (SCLC) is observed when an Ohmic contact (no net electric field at the contact) is assumed and when an injection barrier at zero field ($\varphi_{b(0)}$) at the electrode-PPV interface of ≤ 0.2 eV is assumed. It was also pointed out that the low charge carrier mobility, typically $\mu= 10^{-10}$ m^2/V, of the PPV-based materials enhances the occurrence of space-charge effects in a polymer light-emitting diode.

In the next paragraph SCLC will be treated in more detail as part of the charge transport in polymer light-emitting diodes.

2.4.2 Charge transport

First of all, it is important to note that no device is perfect and that there is always a leakage current in a polymer light-emitting diode determined mainly by processing and technology and not necessarily by the properties of the LEP itself. This leakage current is usually ohmic, i.e. it shows a linear dependence on voltage, and is symmetrical around zero applied voltage. The current observed for double-carrier devices, which have a V_{BI} larger than

zero in contrary to unipolar devices ($V_{BI} \approx 0$ V), below the built-in voltage is also a leakage current. Good polymer light-emitting diodes show a rectification ratio, i.e. ratio of the forward and reverse current, of 10^6. Good power efficiency requires a low leakage current.

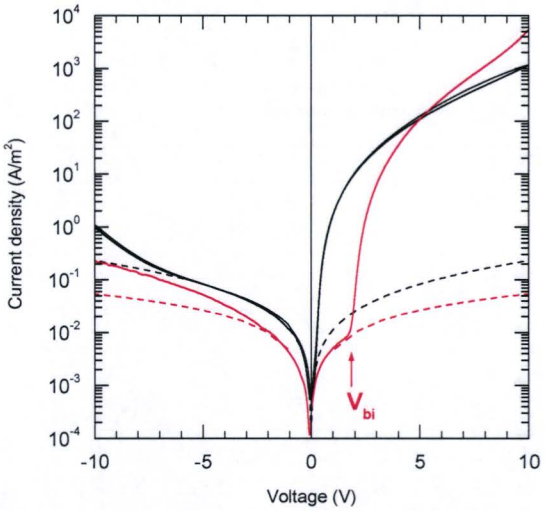

Figure 2.13 A current density-voltage (*J-V*)-plot of a hole-only PolyLED (black colored) and a bipolar PolyLED (red colored) with PPV-derivative as LEP. The dashed lines are in both cases the symmetrical (around $V = 0$ V) leakage current densities. V_{BI} of the bipolar device is 2.1 V and of the unipolar device is 0.1 V.

It has already been mentioned that the observed current above the built-in voltage in a polymer light-emitting diode is of a SCLC nature. This can be understood as a limitation of the charge carrier density due to an inhomogeneous distribution of charge in the LEP. In addition a polymer light-emitting diode can be regarded as a capacitor: Au and ITO (in combination with PEDOT:PSS) are then the electrodes and the LEP the dielectric. At zero bias no current flows and hence no charges are present. For increasingly positive bias more holes are injected, and a higher charge density is obtained. Actually, the maximum charge Q that can be present in a capacitor equals $V \cdot C$, where C is the capacitance. Since the current is simply the ratio of charge and transit time ($I=Q/t$), the capacitive nature of the polymer light-emitting diode defines a maximum current, which is the SCLC. So, the free holes represent a space charge, which is defined as a net charge present in some part of the material. The exact amount of charge in the device is determined by the device area, the dielectric constant of the LEP, the applied voltage, and the average distance between positive and negative charge. According the simplified theory for a trap-free insulator diode [50] one can develop from the Maxwell equations [51] an expression for the SCLC, of which a derivation is given in Appendix A and is called the trap-free square law or the Mott-Gurney square law:

$$J = \tfrac{9}{8}\varepsilon\mu\frac{V^2}{L^3} \qquad (2.4)$$

This is the expression for a hole-only device in which ε is the permittivity, μ is the mobility of the holes and L is the thickness of the LEP layer. This equation is fitted on data obtained from a *J-V* measurement of a typical hole-only polymer light-emitting diode with an 85 nm thick PPV-derivative as LEP to see how it matches, *vide infra*.

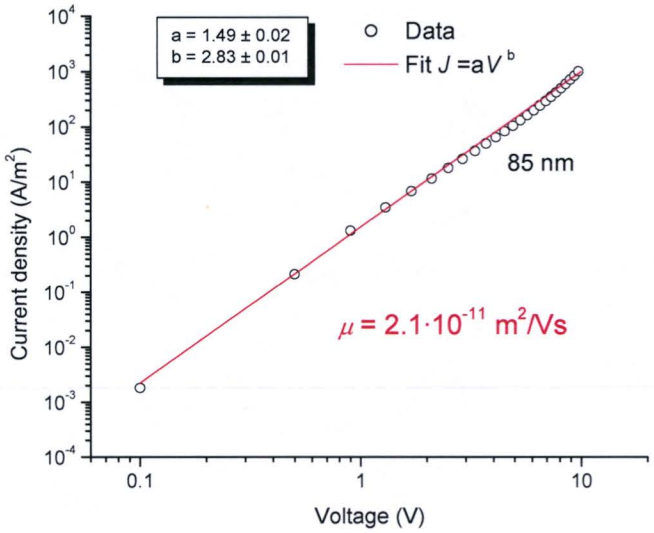

Figure 2.14 A *J-V* measurement of a hole-only PolyLED device consisting of an 85 nm thick LEP layer (black dataset). A fit (red line) of equation $J = aV^b$ has been applied to the dataset resulting in a slightly different exponent (b) than 2 and a hole-mobility of 10^{-11} m^2/Vs.

The measured data match the SCLC predictions reasonably; the discrepancy in the exponent arises from the fact that an actual device does not behave perfectly according the SCLC theory. There are a lot of imperfections, of which traps are the most important one, that ensure that the behavior of a PolyLED deviates from the ideal case. The hole-mobility obtained from the fit is lower than the typical value of 10^{-10} m^2/Vs given in literature. One could also see this as a proof of the presence of traps, of which a definition will be given further on. At much higher voltages (above 10 V) the behavior of a polymer light-emitting diode deviates even more from a simple SCLC behavior. The measured current exceeds the predicted one from SCL-theory. This can be interpreted as a field dependence of the hole mobility. The field and temperature dependency of the mobility is given by the empirical expression derived by Gill [10] in 1972:

$$\mu_P(E,T) = \mu_0 \exp\left[-\frac{\Delta}{kT} + B\left(\frac{1}{kT} - \frac{1}{kT_0}\right)\sqrt{E}\right] \tag{2.5}$$

where Δ, B and T_0 are material properties. Δ is an activation energy typically about 0.4-0.6 eV and $B(1/kT-1/kT_0)$, often indicated as γ, defines an inverse localization length, which is the

"spatial extension" of the energy level. This relation is quite universal, because it describes charge transport in several conjugated polymers, and even doped polymers.

The "universal" dependence of Equation (2.5) has been explained by hopping of charge carriers from one state to the next due to the presence of structural and energetic disorder in the conjugated polymer, i.e. different energy states exist with various energies. This is fundamentally different from crystalline conductors or metals, where the hopping takes also place in delocalized energy bands, but the wavefunctions for the holes and electrons extend over many atoms. On the other hand, wavefunctions of charge carriers in LEPs have an extension of typically 1 nm, thus necessitating many jumps to neighboring positions for transport of a carrier through the device. The details concerning the kinetics of hopping will not be discussed

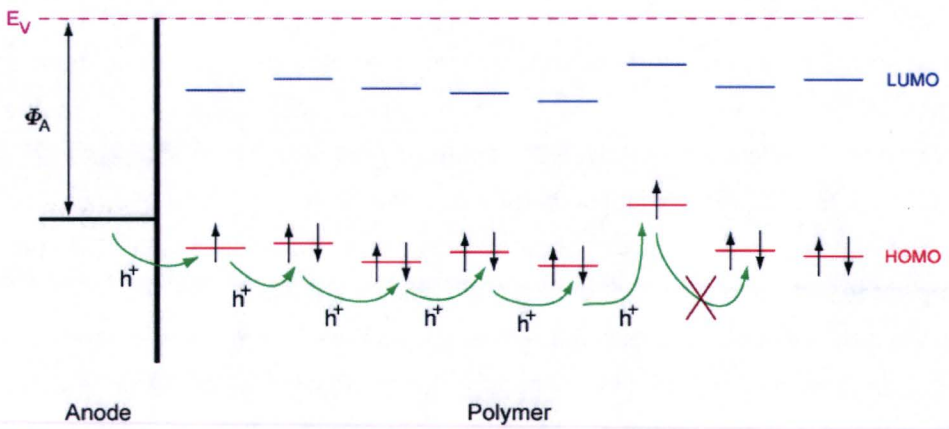

Figure 2.15 The hopping of a charge carrier (holes in this case) from one adjacent site to the other is visualized in the presence of a trap.

Some levels can be of considerably lower energy than adjacent levels. A jump to a neighboring site is then rather unlikely, because such hopping would be an uphill process in energy. Further away, levels with similar energy might be available, but hopping over a longer distance is also highly improbable. Consequently, the charge carrier is trapped. Charge transport in systems with many traps is slowed down markedly compared to the trap-free case. Examples of traps are polymer segments with extreme conjugation length, and impurities introduced in e.g. synthesis or processing. Traps can also be added on purpose: luminescent dyes in host polymers can be viewed as traps.

Another consequence of hopping is so-called dispersive transport: slow and fast routes are available for carrier transport due to the disorder in the LEP. Hence, a spread of velocities with which charge carriers move through the device is achieved. An interesting consequence is that the mobility, which is a material property, apparently becomes dependent on the thickness of the LEP in time-of-flight (TOF) experiments [2]. The reason for this is that in a very thin device there is a bigger chance that a very fast route for charge carriers exists. So, for very thick LEP layers, a transition from dispersive to nondispersive charge transport occurs. Note that the steady-state or dc mobility is still independent of LEP thickness.

In the next paragraph the last process that influences the device operation of a polymer light-emitting diode viz. recombination process of an exciton will be dealt in more detail.

2.4.3 Recombination

Exciton formation by electrostatic or Coulomb interaction between oppositely charged carriers, i.e. free electrons and holes, has already been discussed earlier. Charge carrier recombination and therefore exciton formation is generally described by Langevin recombination [52], which is explicitly spin-independent resulting in a singlet to triplet ratio of 1:3. However, as it has been reported that the number of singlet excitons generated can be larger than 25 %, the Langevin description could be incomplete. This shows that the process that determines the efficiency of PolyLEDs is currently not understood satisfactorily.

Exciton recombination can be comparable to a situation of diffusion-controlled kinetics: the hopping distance of electron and hole are considerably smaller than the distance over which they start to feel the mutual Coulomb interaction, hence the rate of exciton formation is determined by the rate with which the carriers can move to each other, which is simply proportional to their mobility. Although, the conversion efficiency of a polymer light-emitting diode is not dependent on the temperature due to the occurrence of Langevin recombination [2], the required voltage for a certain conversion efficiency increases with decreasing temperature due to the decreasing charge carrier mobility. So, as a result of these two effects a polymer light-emitting diode fabricated with low carrier mobility will only provide sufficient conversion efficiency at high voltages. Hence, this will give rise to poor power efficiency.

3 Experimental techniques & setup

In the first paragraph of this chapter an overview is given of the different devices and (conjugated) polymers used in this research. In the second paragraph the steady-state current density-voltage (*J-V*) measurement technique will be presented. The third and last paragraph will deal with electrical impedance spectroscopy, which is the most-frequently used experimental technique for the research presented in this report.

3.1 Devices

During this research project two kinds of devices were used: pre-pilot line devices and research devices. Both devices were fabricated in a similar manner under clean room conditions. Pre-cleaned ITO coated glass substrates were treated in a UV/O_3 photoreactor and remaining dust particles were blown away with ionized nitrogen. Next, a layer of PEDOT:PSS was spin-coated using a BLE Delta 20 BM, after which it is annealed at 180 °C for 2 minutes. Hereafter, the polymer solution was filtered through a 5 µm filter and was spin-coated with the same apparatus on top of the PEDOT:PSS layer. The devices were then immediately transported to a glove box with a nitrogen atmosphere ($[O_2]$ and $[H_2O] < 1$ ppm), where the metal cathodes were applied by means of vacuum evaporation through a mask. The metal cathodes consisted either out Au (work function of 5.3 eV [53]) or Ba/Al (work function of 2.7 eV [53]) depending on whether, respectively, a unipolar or bipolar device was desired.

The pre-pilot line device is neatly encapsulated with a metal lid to prevent oxygen and water from degrading the device performance. Moreover, a getter is included in the encapsulated device. On the other hand, the research device has to be measured immediately after transfer from the glove box and the measurement time must be kept short so that the measurement does not suffer from oxidative degradation of the polymer [54].

Another difference between those two is the layout of the pixels on the devices. The pre-pilot line devices were ordered in batches. Each batch consists of three plates (A, B and C) and each plate contains nine devices. Each pre-pilot line device consists of one large 2x3 cm^2 pixel (also called backlight), three 3x3 mm^2 pixels, three 1x1 mm^2 pixels and three 0.3x0.3 mm^2 pixels. All pixels except the backlight have a common cathode. The ITO anode on the other hand is patterned so as to define the various pixel dimensions. There are contact leads from the rim of the device to all these ITO structures in order to contact the different pixels. For our measurements, only the three 3x3 mm^2 pixels were used and were designated as first pixel (fp), middle pixel (mp) and last pixel (lp). These pixels are depicted in.

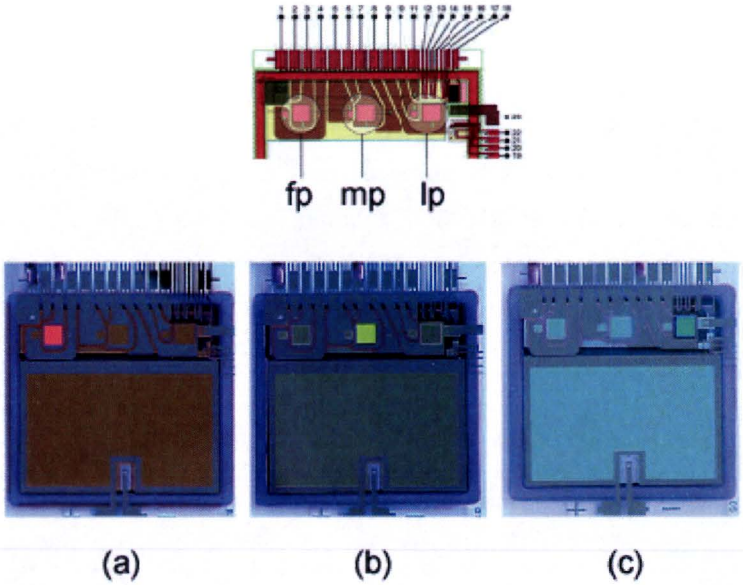

Figure 3.1 A picture of a pre-pilot line device in the case that the three 3x3 mm pixels fp (a), mp (b) and lp (c) are emitting light under application of a bias voltage larger than V_{BI}.

The smaller pixels were not measured because the diode area compared to the area of the contact leads is very small and therefore it has relatively large parasitic components. The backlight was not measured because the outcome would almost certainly suffer from layer inhomogeneities due to the large area of this diode.

Each research device has four pixels: 3x3 mm^2, 4x4 mm^2, 6x6 mm^2 and 1x1 cm^2. These pixels are located at the cross sections of the ITO and cathode structures and are named diode 1 (D1), diode 2 (D2), diode 3 (D3) and diode 4 (D4), respectively, as it is depicted in Figure 3.2.

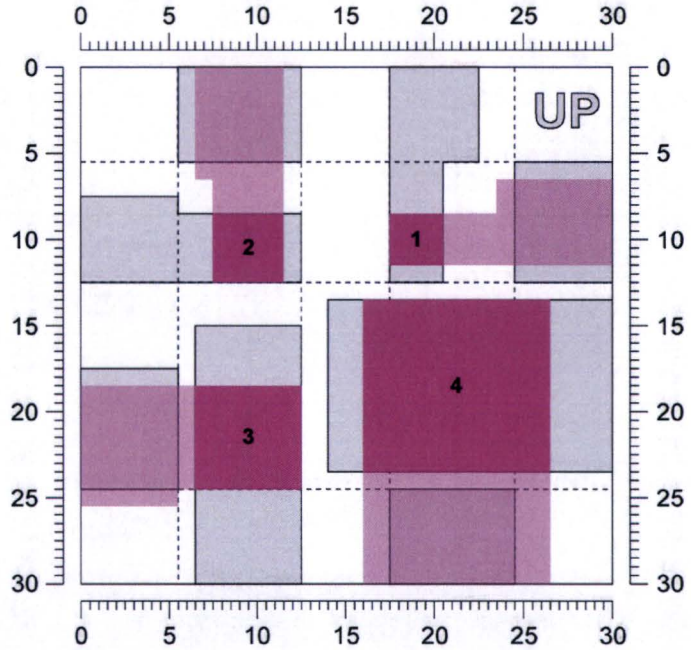

Figure 3.2 Research device layout in which the ITO structures (gray) and the cathode structures (light and dark purple) are depicted. The various pixels (diodes) are located at the cross sections of these structures (dark purple) and are numbered from 1 to 4 with increasing pixel area. The dimensions are given in mm.

Of the research devices only the first and second diodes are measured, because the other two pixels (especially the largest one) regularly show layer inhomogeneities that could influence the outcome of the measurements.

In both pre-pilot line as research devices several parameters such as type of LEP (PPV, PSF or PFO), type of HTL (PEDOT:PSS), resistivity and ion concentration of HTL, LEP thickness, HTL thickness were varied or an external stimulus (UV, heat, high voltage) was applied and the effect of these on the behavior of PolyLEDs was studied with electrical impedance spectroscopy.

3.2 Steady-state current density-voltage experiments

Steady-state current density-voltage (*J-V*) measurements were performed by applying a time-independent voltage for a certain step time (usually 1 s) after which the applied voltage is increased/decreased with steps of typically 0.05 V. The current density-voltage measurements have been performed in a glove box (nitrogen atmosphere) or in ambient atmosphere depending on whether a research device or a pre-pilot line device was used in the experiments. The *J-V* measurements in ambient atmosphere have been performed with a HP 4245A semiconductor parameter analyzer, while the *J-V* measurements in the glove box

have been performed with a Keithley 2400 SourceMeter®. In both cases, the equipment was driven and controlled by custom-made Labview software.

As can be seen in Figure 2.13, the electronic response of a unipolar (hole-only) device is quite different than that of a bipolar device. Moreover, the built-in voltage (V_{BI}) can be deduced from the *J-V* plot.

3.3 Electrical impedance spectroscopy

Electrical impedance spectroscopy (EIS) is a powerful method for characterizing many of the electrical properties such as mobility, conductivity, dielectric constant, etc. of conjugated polymers and their interfaces with electrodes and/or charge-injection layers. Any intrinsic property or external stimulus that influences the conductivity of a conjugated polymer-electrode interface can be studied by EIS. Therefore it is widely used to understand the functioning of e.g. PolyLED devices and to correlate physical and chemical processes to the observed electronic behavior.

EIS is only meaningful and useful in linear systems in which an application of the first harmonic (sinus signal) results in negligible generation of higher harmonics. Although most real systems are nonlinear, EIS can still be used when the applied RMS voltage amplitude (V_m), is equal to or less than the thermal voltage $V_T = RT/F = kT/e$, which is about 25 mV at 25 °C. In this case, the basic differential equations governing the response of the system become linear to an excellent approximation [55]. In other words, the current is directly proportional to the applied voltage. From the various approaches to EIS the most common and standard one, as will be explained below, has been used in this research.

First, the pre-pilot line device is mounted on a device holder, which is attached to a Schlumberger SI 1260 impedance/gain-phase analyzer. In addition, research devices have to be measured in a vacuum box to prevent the LEP from degrading.

For a typical EIS measurement, the input signal consists of a sinusoidally time-varying voltage modulation (with amplitude V_m) superimposed on a constant background voltage (V_0). Input parameters that can be varied are the background voltage and the angular frequency of the voltage modulation (ω).

$$V(t) = V_0 + V_m \sin(\omega t) \tag{3.1}$$

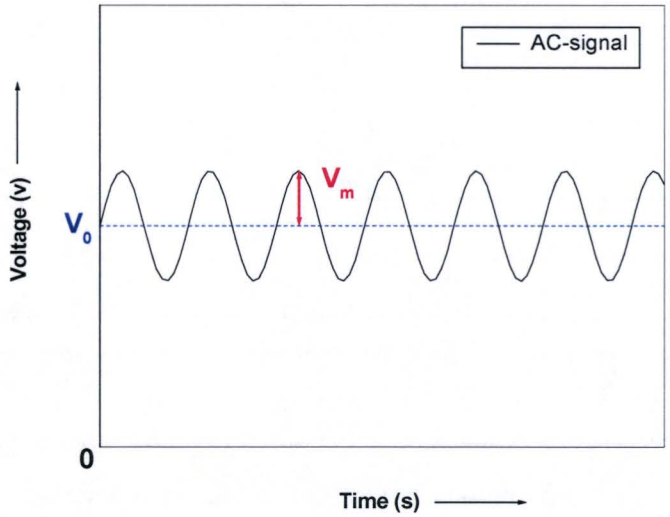

Figure 3.3 The AC-voltage signal as a function of time used to conduct impedance measurements.

As a result of the applied voltage a current flows in the device. Generally, the current is phase-shifted by an angle θ with respect to the applied voltage, which indicates the presence of capacitive and/or inductive processes in the device.
The impedance (Z), which is the total passive opposition offered to the flow of electric current, is defined as the ratio between the applied voltage $V(t)$ and the resulting current $I(t)$:

$$z = \frac{V(t) - V_0}{I(t) - I_0} \tag{3.2}$$

Formally, the impedance is a complex quantity, of which the real part is called resistance (R) and of which the imaginary part is called reactance (X), both in units Ω.

$$z = R + iX \tag{3.3}$$

The modulus of the impedance ($|Z|$) and the phase angle (θ) are given by:

$$|Z| = \sqrt{R^2 + X^2} \text{ and } \theta = \arctan\left(\frac{X}{R}\right) \tag{3.4}$$

For a capacitor, the reactance (X_C) is given by:

$$X_C = \frac{1}{\omega C} \tag{3.5}$$

The reciprocal of the impedance is called the admittance (Y), which describes the ease with which electric current can flow. The admittance is also a complex number, of which the real part is called conductance (G) and the imaginary part susceptance (B), both in units S.

$$Y = \frac{1}{Z} \text{ and } Y = G + iB \tag{3.6}$$

When dealing with circuit elements that are connected in series, the concept of impedance is used, as this is mathematically more straightforward. Conversely, the admittance is used when dealing with circuit elements that are connected in parallel.

Now, let us see how impedance spectroscopy has been utilized in our experiments. First, measurements were performed at a constant background voltage while the voltage modulation frequency was varied from 10 Hz to 10^6 Hz. The obtained data are plotted in a Bode plot, i.e. the modulus of the impedance and the phase angle are plotted as function of the frequency f, which is equal to $\omega/2\pi$. For a pure capacitor one would observe a phase angle of $-\frac{1}{2}\pi$ over the whole frequency range and the slope in the $|Z|$-f plot would be −1. The presence of a resistor in series with the capacitor (i.e. a contact resistance) will manifest itself at high frequencies (10^5 Hz – 10^6 Hz). The presence of a resistor parallel to the capacitor will manifest itself at low frequencies. When the frequency sweep is performed at 0 V (i.e. below V_{BI}) the device usually behaves as a pure capacitor with a small contact resistance.

In general, a polymer light-emitting diode can be characterized by an equivalent circuit as shown below.

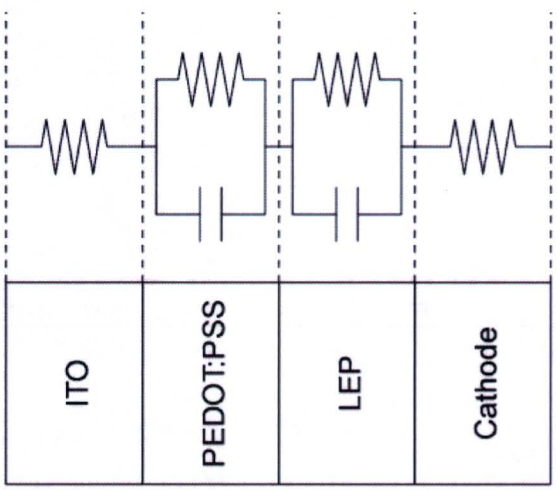

Figure 3.4 An equivalent circuit characterizing the behavior of a polymer-light emitting diode. Note that the PEDOT: PSS layer is modeled as a separate parallel *RC*-circuit.

The anode (ITO) and cathode (Au or Ba/Al) are represented by a resistance, while the two organic layers (PEDOT:PSS and LEP) are represented by parallel RC elements.

Depending on the type of PEDOT:PSS, the above equivalent circuit can be simplified. When the PEDOT:PSS used has a low resistivity (low-Ω PEDOT:PSS), the parallel RC element that represents this layer reduces to a resistance only (at least, within a frequency range of 10 Hz to 10^6 Hz). This means that a device that contains low-Ω PEDOT:PSS can be described by the simplified equivalent circuit shown below.

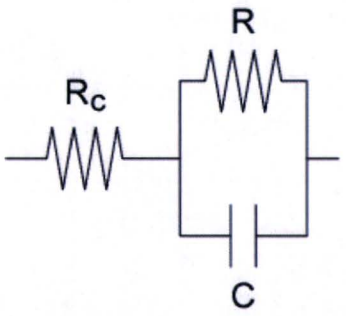

Figure 3.5 An equivalent circuit used to characterize the polymer-light emitting diode in the case of a low-Ω PEDOT:PSS. R_c represents a contact resistance.

Here, R_c stands for contact resistance and it incorporates the resistance of the electrodes and the PEDOT: PSS layer (and of the cables, etc.), while R and C are the (differential) resistance and capacitance of the LEP layer respectively. When a value for R_c is known, the measurement can be corrected for this component to yield the signal originating from the LEP layer only. A value for R_c can easily be extracted from a frequency sweep that is performed at a voltage above the built-in voltage of the device. At such a voltage, the value of R has decreased to such an extent that for a frequency range of 10 Hz to 10^6 Hz the impedance shows a clear semicircle in the complex plane that can be fitted with a software program called ZView[††] to the above equivalent circuit.

[††] Zview: version 2.4a, Scribner Associates, Inc.

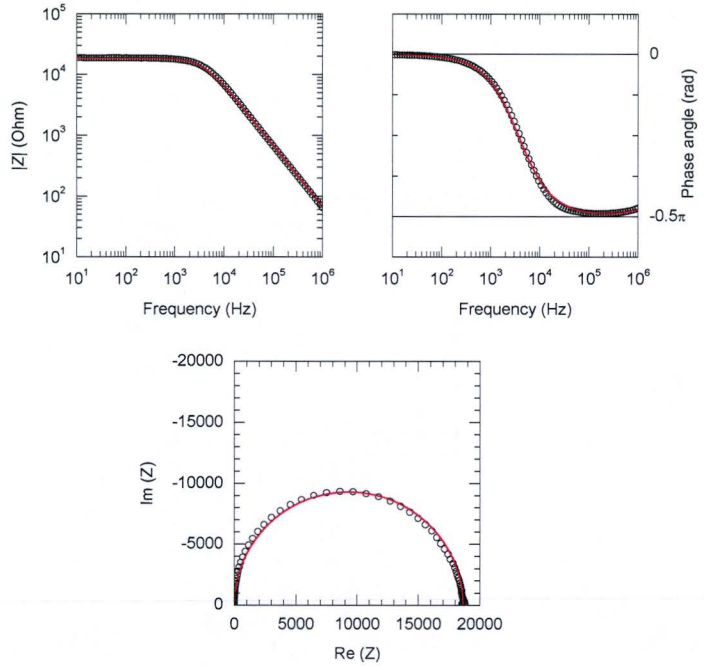

Figure 3.6 Bode plots (upper two) and Nyquist plot (lower one) of data (black data points) obtained from a frequency sweep at a background voltage of 3 V are shown. A fit (red line) using the equivalent circuit of Figure 3.5 yields typical values of 10 Ω for R_C, 2 nF for C and 1 MΩ for R.

An interesting parameter is the capacitance of LEP layer. Of course, a value for this capacitance can also be obtained from the same frequency sweep as described above. However, this procedure assumes a frequency-independent capacitance. Alternatively, the capacitance can be determined at a fixed frequency by performing a voltage sweep. Using the simplified equivalent circuit shown above, when the admittance (Y) is corrected for R_c, it is given by:

$$Y = \frac{1}{R} + i \cdot \omega C \tag{3.7}$$

This means that the ratio of the imaginary part of Y and the angular frequency ($\mathrm{Im}(Y)/\omega$) is equal to the capacitance. For a typical device containing low-Ω PEDOT:PSS, when the measurement is performed at a high frequency ($f = 10^6$ Hz), a constant value is obtained when $\mathrm{Im}(Y)/\omega$ is plotted versus the applied voltage. This value is equal to the geometrical capacitance (C_0) of the LEP layer at that particular frequency.

$$C_0(\omega) = \varepsilon(\omega) \cdot \frac{A}{d} \tag{3.8}$$

Whilst, a voltage sweep at low frequency (f = 10 Hz) captures the charge transport processes occurring on time scale τ, which is $\sim \omega^{-1}$, hereby unraveling the slow dynamical processes in a polymer light-emitting diode.

So, impedance spectroscopy has been used successfully within this research framework to obtain and interpret the observed impedance behavior and hereby correlating it to physical or chemical processes occurring on different time scales in a polymer light-emitting diode.

4 Results and discussion

In this chapter all the features present in the electrical impedance behavior of a polymer light-emitting diode are described and discussed step by step. First starting with an insulating inert polymer Zeonex®, proceeding with PPV and finishing with PFO and PSF. Furthermore, devices with and without a PEDOT:PSS layer have been measured.

4.1 An inert insulating polymer: Zeonex®

As a first step into the understanding of polymer light-emitting diodes research devices with only a 210 nm layer of an inert isolating polymer have been analyzed with EIS. This polymer is the commercially available cyclo-olefin homopolymer Zeonex® type 180s (Zeon Chemicals L.P.), which has a relative dielectric constant (κ) of 2.27 at 1 MHz.

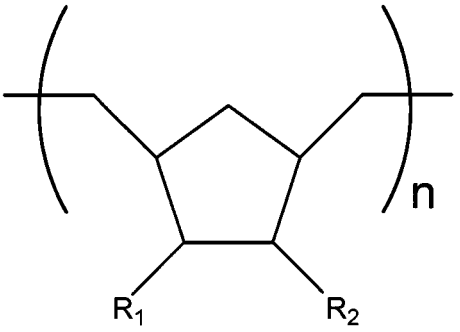

Figure 4.1 The chemical structure of the cyclo-olefin homopolymer Zeonex®.

It is expected that this device will behave like a parallel-plate capacitor. The results are given below.

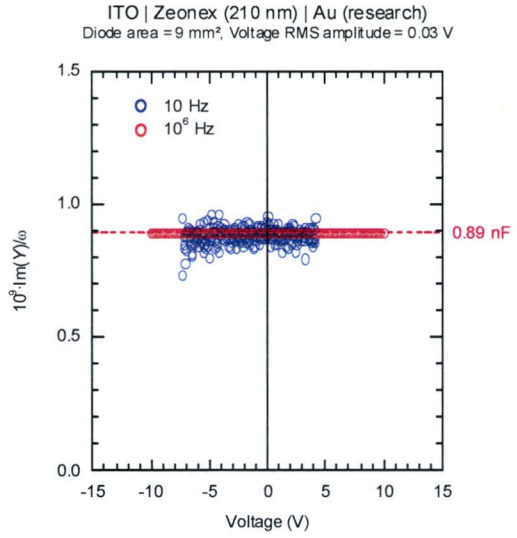

Figure 4.2 The capacitance of an ITO-Zeonex® (210 nm)-Au device expressed as the imaginary part of the admittance divided by the angular frequency plotted as a function of the applied bias voltage at frequencies of 10 Hz and 1 MHz The integration time was set at 1 s and V_m at 0.03 V. The diode area is 9 mm^2.

At 1 MHz, a voltage-independent capacitance of 0.89 nF is measured. Using Equation 3.8, this measured value translates to a relative dielectric constant of 2.34, which is in good agreement with the literature value of 2.27. Although at 10 Hz the signal-to-noise ratio of the measurement is not as good as at 1 MHz, it is clear that at this frequency also a voltage-independent capacitance is measured, having a similar value as obtained at 1 MHz. This means that the relative dielectric constant of Zeonex® 180S is constant over a frequency range of 10 Hz to 1 MHz.

What would happen if a PEDOT:PSS layer is introduced into this device? A high-resistivity PEDOT:PSS, referred to as JOF 5526-14, containing 1500 ppm Na^+ has been used for this purpose. The thickness of the PEDOT:PSS layer is 140 nm. The EIS result for this research device is given below.

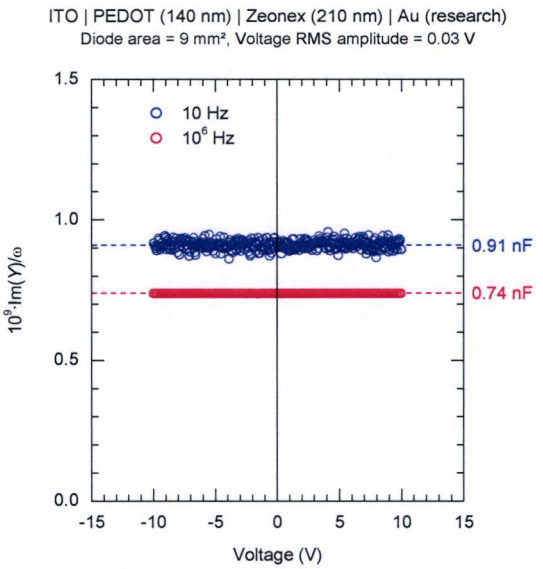

Figure 4.3 The capacitance of an ITO-PEDOT:PSS (140 nm)-Zeonex® (210 nm)-Au device expressed as the imaginary part of the admittance divided by the angular frequency plotted as a function of the applied bias voltage at frequencies of 10 Hz and 1. The PEDOT:PSS used was the high-resistivity JOF 5526-14. The integration time was set at 1 s and V_m at 0.03 V. The diode area is 9 mm^2.

The value obtained from the measurement at 10 Hz in Figure 4.3 is close to the value of the geometrical capacitance 0.89 nF in Figure 4.2. However, the measurement at 1 MHz now yields a value of 0.74 nF that is significantly lower than 0.89 nF. If the value measured at 1 MHz represents the geometrical capacitance of a Zeonex® layer, this layer would have to be 244 nm thick, instead of the requested 210 nm. This difference is too large to be accounted for by a difference in device preparation. A more probable explanation would be that at 1 MHz the effective capacitance of a serial combination of two capacitances is measured, one capacitance representing the Zeonex® layer while the other one represents the PEDOT:PSS layer. Based upon this equivalent circuit a relative dielectric constant of approximately 9 has been calculated for JOF 5526-14 at 1 MHz.

The value measured at 10 Hz is close to the geometrical capacitance of the Zeonex® layer. This could mean that at 10 Hz, the capacitance of the PEDOT:PSS layer is much larger than that of the Zeonex® layer, and only the latter is effectively measured. If this is the case, the relative dielectric constant of the PEDOT:PSS layer should have increased strongly upon going from 1 MHz to 10 Hz. This particular feature will be discussed later in this chapter, following the presentation of some extra results.

Several other research devices with varying PEDOT:PSS layer thicknesses have been analyzed with EIS. From the 1 MHz results effective capacitances have been determined while presuming a polymer layer thickness of 210 nm and a PEDOT:PSS layer thickness of 140 nm. These values have been plotted as a function of the PEDOT:PSS layer thickness (*vide infra*).

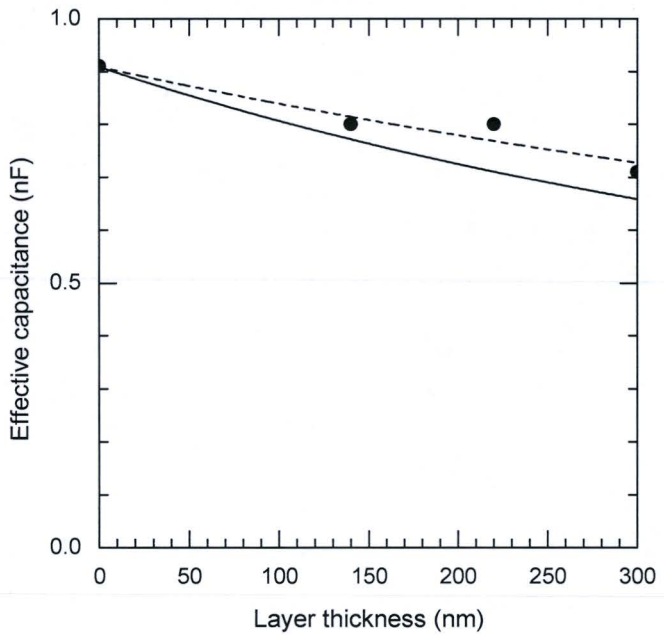

Figure 4.4 The solid circles are the measured effective capacitances. These values have been plotted as a function of the PEDOT:PSS layer thickness. The solid line is the PEDOT:PSS layer thickness dependence as expected when PEDOT:PSS has a relative dielectric constant of 9 at 1 MHz (see above). The dashed line is a fit that results in a relative dielectric constant for PEDOT:PSS of 13.8 at 1 MHz.

The solid line in Figure 4.4 is the PEDOT:PSS layer thickness dependence as expected when PEDOT:PSS has a relative dielectric constant of 9 at 1 MHz (see above). The dashed line Figure 4.4 is a fit that results in a relative dielectric constant for PEDOT:PSS of 13.8 at 1 MHz. So, it seems that the relative dielectric constant of PEDOT:PSS has a value somewhere between 9 and 14.

In the next paragraph our focus will shift from Zeonex® to the PPV-derivative called Super Yellow (SY), and the accompanying effects will be described.

4.2 PPV-derivative as polymer and no PEDOT:PSS layer

The polymer that has been used is referred to as Super Yellow (SY) and is a PPV copolymer with different R_1 and R_2 side groups (depicted in Figure 1.3). This polymer will emit yellow light (577 – 597 nm) when used in a bipolar PolyLED. Pre-pilot line devices of this polymer have been analyzed with EIS. The data have been visualized in 3D-plots (vide infra).

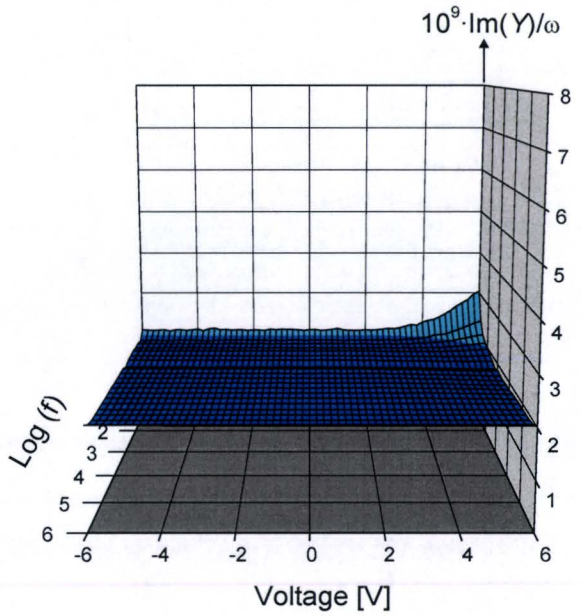

Figure 4.5 The capacitance of an ITO-SY (150 nm)-Au device expressed as the imaginary part of the admittance divided by the angular frequency plotted as function of both the logarithm of the frequency and the applied bias voltage.

One immediately observes that the capacitance of this diode is approximately 2 nF over the whole frequency and voltage domain, except at the low frequency-high forward bias voltage domain. The increase of the capacitance with decreasing frequency and increasing voltage in this domain can be attributed to SCL current transport, as has been pointed out in paragraph 2.4.2. Now, a cross-section at 10 Hz and 1 MHz has been taken from Figure 4.5 and plotted together in the next figure.

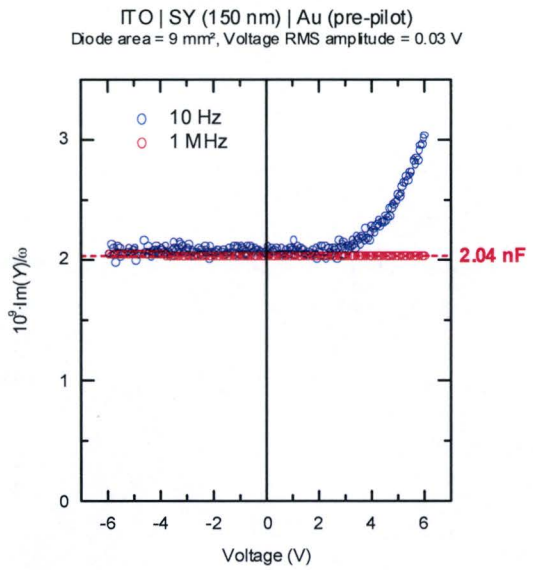

Figure 4.6 The capacitance of an ITO-SY (150 nm)-Au device expressed as the imaginary part of the admittance divided by the angular frequency plotted as a function of the applied bias voltage at a frequency of 10 Hz and 1 MHz. The integration time was set at 1 s and V_m at 0.03 V. The diode area is 9 mm^2.

From the voltage-independent capacitance at 1 MHz, a relative dielectric constant of 3.8 is calculated for SY. In fact, this value is somewhat larger than the value usually measured for PPV derivatives ($\kappa = 3.1$) which could mean that the actual thickness of the SY layer in this particular device is slightly lower than 150 nm.

If the low-frequency data from Figure 4.6 are compared to those in Figure 4.2, then one can observe a built-in voltage for the SY device, above which the capacitance increases with increasing applied voltage. This is due to the fact that SY shows semiconducting behavior. The capacitance increase arises from SCLC as pointed out earlier. Already, in Figure 2.14 it was pointed out that SCLC-theory applied on data obtained from a *J-V* measurement on a similar device yields a hole-mobility of $2 \pm 1 \cdot 10^{-11}$ m^2/Vs, which is in reasonable agreement with typical values of 10^{-10} m^2/Vs reported in literature [2].

The logical next step towards enlarging our understanding of polymer light-emitting diodes is to add a PEDOT:PSS layer and to observe the additional effects that show up as a result of this.

4.3 PPV-derivative as polymer and a PEDOT:PSS layer

In order to detect any additional features introduced by the presence of a PEDOT:PSS layer, EIS has been performed on devices containing a layer of SY on top of a PEDOT:PSS layer. The PEDOT:PSS in question is a low-resistivity PEDOT:PSS containing approximately 75 ppm Na^+ and is referred to as PEDOT 5792/P2. The result for this device is given below in Figure 4.7.

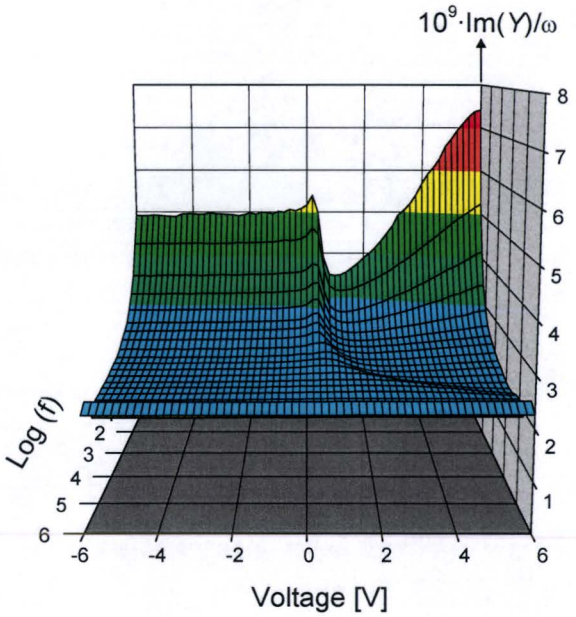

Figure 4.7 The capacitance of an ITO-PEDOT:PSS (150 nm)-SY (120 nm)-Au device expressed as the imaginary part of the admittance divided by the angular frequency has been plotted as function of both the logarithm of the frequency as the applied bias voltage. The PEDOT:PSS used is the low-resistivity PEDOT:PSS 5792/P2.

With respect to the device containing only a SY layer (see Figure 4.5), two additional features can be observed at low frequencies: the peak at V_{BI} and a shift of the voltage-independent capacitance as observed under reverse bias to higher values. Moreover, the increase in capacitance due to SCLC in forward bias is stronger than was observed for a device containing only a SY layer (see Figure 4.5). However, all of these extra features disappear when the voltage modulation frequency is increased to 1 MHz. At 1 MHz, the geometrical capacitance of the SY layer is measured. In Figure 4.8 cross-sections of Figure 4.7 at 10 Hz and 1 MHz are given together with the different regions representing the various features.

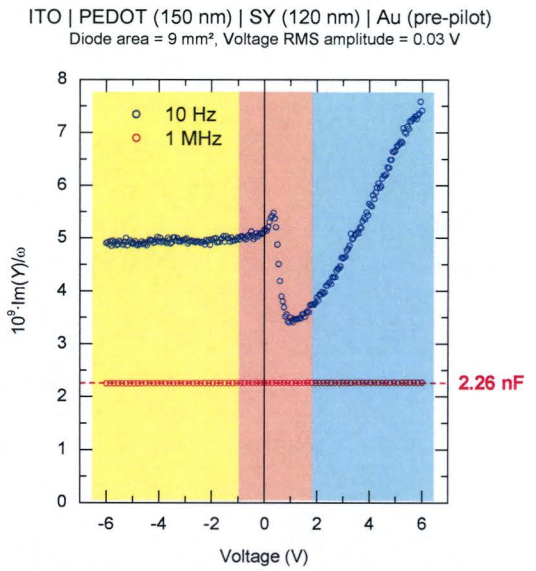

Figure 4.8 The capacitance of an ITO-PEDOT:PSS (150 nm)-SY (120 nm)-Au device expressed as the imaginary part of the admittance divided by the angular frequency plotted as a function of the applied bias voltage at a frequency of 10 Hz and 1 MHz. The PEDOT:PSS used was the low-resistivity PEDOT:PSS 5792/P2. The integration time was set at 1 s and V_m at 0.03 V. The diode area is 9 mm^2. The reverse bias region is colored yellow, the peak-region is colored pink and the SCLC region is colored blue.

The different regions that can be observed in Figure 4.8 are: the forward bias region with its SCLC nature (blue colored), the region around V_{BI} with a peak (pink colored) and finally the reverse bias region (yellow colored). These three regions, respectively, will be treated separately in the following subsections.

4.3.1 The forward bias region

Already, in paragraph 2.4.2 this region was discussed and the qualitative analysis pointed at a space-charge limited (SCL) behavior. In a first analysis, trap-free SCL behavior was assumed for a device containing only a LEP layer and the Mott-Gurney square law (Equation (2.4)) was used to calculate a hole-mobility from a power-law fitted to the forward bias region (see Figure 2.14). The fit yielded a power-law dependency of 2.8 between the current density and the voltage instead of 2, which would be the case if it behaved according to trap-free SCLC theory. Usually, a power-law dependency J-V^m with $m > 2$ is attributed to the presence of traps in the LEP layer, having an exponential distribution [8, 56]. One can use the trap-filled limit SCLC (TFL-SCLC) theory [50] to extract information about the material such as trap-density (N_t). A brief summary of TFL-SCLC is given in Appendix B.

J-V measurements have been performed at room temperature (293 K) on unipolar (hole-only) devices containing a SY layer (85 nm) on top of a PEDOT:PSS layer (120 nm). The logarithm of *J* has been plotted as a function of the logarithm of *V* in Figure 4.9 for the forward bias region.

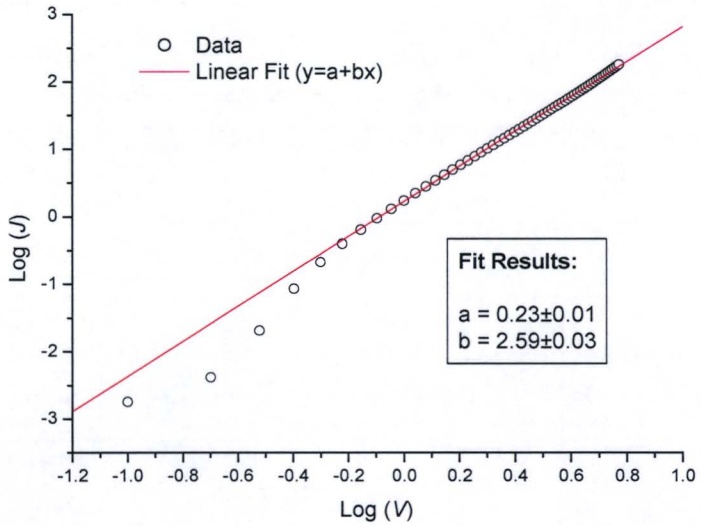

Figure 4.9 The logarithm of *J* plotted as a function of the logarithm of *V* for the forward bias region (open circles) as measured on an ITO-PEDOT:PSS (120 nm)-SY (85)-Au device. A linear fit according to Equation (B.5) has been applied (red line) for log(*V*) between {0, 1}; the fit spans the whole X-axis.

According to Equation (B.5) and the fit results, $l+1$ is equal to 2.59 ± 0.03. Using Equations (B.2) and (B.1), the characteristic energy E_t is calculated to be 0.04 eV at room temperature. This parameter is directly related to the steepness and depth of the exponential trap distribution, a smaller value indicating a much steeper distribution close to the upper level of the valence band [57]. So, for the device described here, the trap levels are close to the valence band levels therefore resulting in a steep exponential distribution of traps. The next question concerns the trap density. To calculate the trap density (N_t) from Equation (B.4) one needs to know two additional parameters: the density of states (N_V) in the valence band and the hole-mobility (μ). Although, the latter was already estimated to be $2 \cdot 10^{-11}$ m^2/Vs (see paragraph 2.4.2) in the case of pure SCLC for a device without PEDOT:PSS, this value has been used to estimate the trap density, because it was otherwise not possible due to two unknown parameters (i.e. μ and N_t). The density of states in the valence band is estimated to be $8 \pm 3 \cdot 10^{26}$ m^{-3} for PPV [57]. So, by inserting these values and the value obtained from the fit into Equation (B.4) one calculates a value for N_t of $8 \pm 2 \cdot 10^{23}$ m^{-3}. Values for N_t reported in literature for similar devices are: $3 \pm 1 \cdot 10^{23}$ m^{-3} [57], $8 \cdot 10^{23}$ m^{-3} [58] and $>2 \cdot 10^{21}$ m^{-3} [59]. So, our estimation of the trap density is in good agreement with values found in literature.

In the above analysis (as conducted by us and the various referenced authors) a constant hole-mobility has been assumed. However, the empirical law of Gill (see Equation (2.5)) predicts a field-dependent hole-mobility. If one defines a normalized hole-mobility (μ^*) defined by μ / μ_0, in which μ_0 is the zero-field mobility, then one can plot the normalized mobility as a function of the bias voltage by using the relationship $E=V/d$. In Equation (2.5) T_0 and B are constants for which the following values have been determined by Blom *et al.* [2] 600 K and $2.7 \cdot 10^{-5}$ eV(V/m)$^{-½}$, respectively. The Boltzmann constant k has a value of $0.862 \cdot 10^{-4}$ eVK^{-1}. At room temperature (293 K) kT is equal to 25 meV and because $T_0 > T$ the second term between brackets is omitted from Equation (2.5). The plot of μ^*-V is given below.

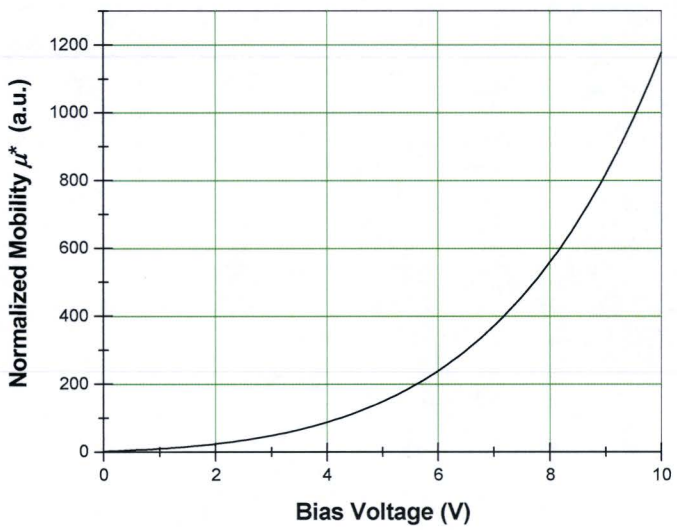

Figure 4.10 The normalized mobility μ^* has been plotted as a function of the bias voltage V of the AC-signal using Equation (2.5) and $E=V/d$.

It is clear that the mobility is actually very sensitive to the applied field: at 10 V it has increased already more than 1000 times. Obviously, this effect has to be taken into account. Recently, it has been reported that there is a strong dependence of the mobility on the charge carrier density [60]. The field-dependence and the charge carrier density-dependence of the mobility have also an influence on the capacitance at 10 Hz at forward bias. Trap-free SCLC with field-independent mobility predicts that the capacitance beyond V_{BI} is a factor 3/2 higher than the value of the capacitance below V_{BI}. The fact that there is not an abrupt increase beyond V_{BI} points at a not constant mobility. The observation that the capacitance becomes eventually higher than 3/2 times C_0 indicates that there are traps present. In the next subsection, the second region (pink colored in Figure 4.8) concerning the region around V_{BI} will be discussed in more detail.

4.3.2 Trapping around V_{BI}

The peak detected around the built-in voltage in Figure 4.7 and Figure 4.8 for devices containing both PPV and PEDOT:PSS is not observed in Figure 4.5 for devices containing only a PPV layer. This indicates that the presence of a PEDOT:PSS layer somehow introduces this feature. However, if one examines Figure 4.3 for a device containing Zeonex® and PEDOT:PSS more closely, one can see that the peak is absent. It is highly unlikely that Zeonex® has had any interaction with PEDOT:PSS due to the nature of Zeonex® (i.e. inert, fully saturated carbon chain). One therefore has to ascribe the presence of the peak to a possible interaction of PPV with PEDOT:PSS. So, merely a presence of a PEDOT:PSS layer is not enough to introduce a peak around V_{BI}, there has to be some interaction between the polymer (in this case PPV) and PEDOT:PSS. To see if this hypothesis is correct a research device has been fabricated which has just a layer of SY that has been "pre-treated" with PEDOT:PSS. This pre-treatment consists of mixing a SY and a PEDOT:PSS solution and stirring this mixture vigorously for 1 h so that both solutions have had plenty of opportunity to interact. After phase separation, part of the organic phase (containing only SY and no PEDOT:PSS) is separated and used to spin coat a layer from. The result of EIS performed on the resulting device is shown below.

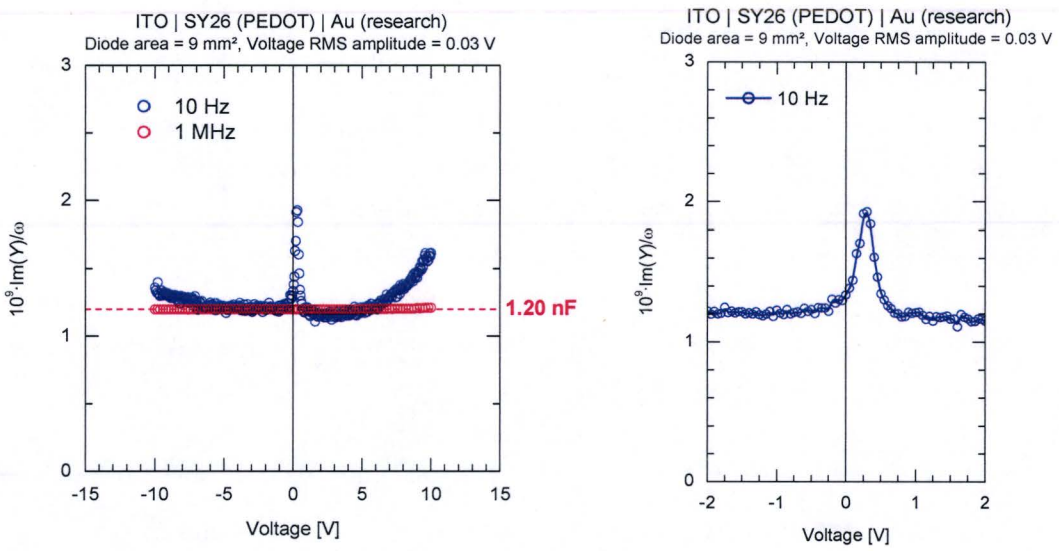

Figure 4.11 The capacitance of an ITO-SY-Au device expressed as the imaginary part of the admittance divided by the angular frequency plotted as a function of the applied bias voltage at a frequency of 10 Hz and 1 MHz. The SY has been pre-treated with PEDOT:PSS. The integration time was set at 5 s and V_m at 0.03 V. The diode area is 9 mm^2. The right graph is a close-up of the peak region.

The result shows that the peak is due to the interaction of PPV with PEDOT:PSS (when compared to Figure 4.6) and not to the mere presence of a PEDOT:PSS layer in the device.

Infrared (IR) spectroscopy and nuclear magnetic resonance (NMR) spectroscopy have been performed on pristine SY and on PEDOT:PSS-treated SY to discover any differences in chemical composition/structure. Unfortunately, the results from these analyses did not indicate any difference in chemical composition and/or structure between the pristine SY and the PEDOT:PSS-treated SY. The exact nature of the interaction between PEDOT:PSS and PPV therefore still remains unclear.

The fact that the increase in capacitance towards a maximum at around V_{BI} is observed at low modulation frequency indicates that the relevant physical process is relatively slow. A process that could be responsible for the occurrence of a capacitance peak is the charging (filling) of traps at the interface of PEDOT:PSS and PPV [61-63]. Although the exact nature of the traps is unclear, they could be defects originating from a chemical interaction between (acidic) PEDOT:PSS and PPV, possibly involving the vinylene bond of PPV [59]. Note that as the devices studied here are hole-only devices, the charge carriers that are trapped at the PEDOT:PSS-LEP interface are holes.

At high frequency, the charge trapping process is unable to follow the rapid electric field modulation and the process is not observed anymore in an EIS measurement. A similar effect is observed when the temperature of the device is lowered [64].

The frequency-dependence of the capacitance peak has been studied, and the peak area is plotted versus the voltage modulation frequency in Figure 4.12.

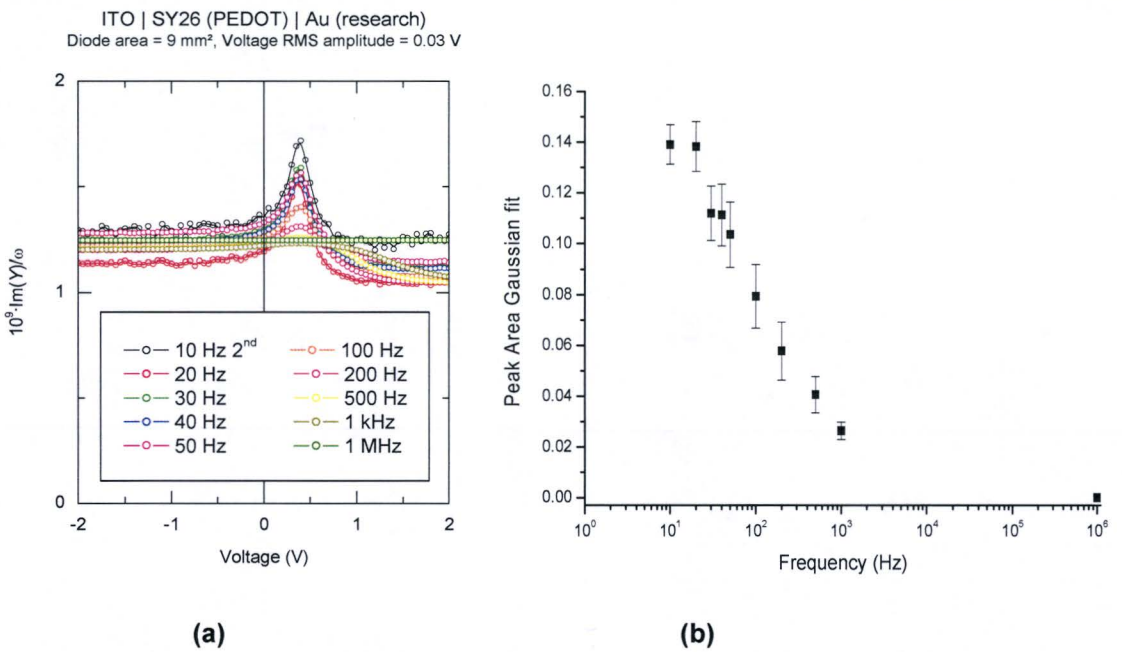

Figure 4.12 (a) The capacitance of an ITO-SY-Au device expressed as the imaginary part of the admittance divided by the angular frequency plotted as a function of the applied bias voltage at modulation frequencies varying from 10 Hz to 1 MHz. The SY has been pre-treated with PEDOT:PSS. The integration time was set at 5 s and V_m at 0.03 V. The diode area is 9 mm^2. (b) The values obtained for the peak areas by applying a Gaussian fit have been plotted as a function of the modulation frequency.

In Figure 4.12 (b) one can observe that the peak area decreases rapidly towards zero for higher modulation frequency; At 1 kHz it is already close to zero. Since the lowest frequency of our measurement is 10 Hz, our measurement is not sensitive to traps that are not in equilibrium on a time scale of 0.1 s. From Figure 4.12 (b) it seems that the peak area saturates toward a frequency-independent value at lower frequency. Note that in Figure 4.12 (a) the second voltage sweep at 10 Hz has been chosen as a starting point for this series of measurements. The reason for this can be explained by looking at two voltage sweeps at 10 Hz performed immediately after each other.

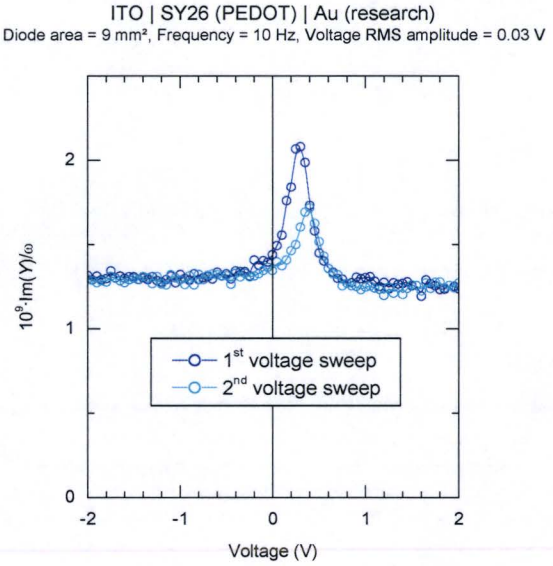

Figure 4.13 The capacitance of an ITO-SY-Au device expressed as the imaginary part of the admittance divided by the angular frequency plotted as a function of the applied bias voltage at a frequency of 10 Hz. The SY has been pre-treated with PEDOT:PSS. The integration time was set at 5 s and V_m at 0.03 V. The diode area is 9 mm^2. The second voltage sweep (cyan colored) has been performed immediately after the first voltage sweep (blue colored).

From Figure 4.13 it is clear that at 10 Hz the peak area of the second voltage sweep is smaller than that of the first sweep. Several subsequent sweeps at 10 Hz after the second one have been performed (not shown here) which indicate that the peak area remains constant after the second voltage sweep. Therefore, the second sweep at 10 Hz has been taken as a reference in the series of measurements exhibited in Figure 4.12 (a). An explanation for the decrease of the peak area in the second sweep could be that some of the (deeper lying) traps are still occupied due to the first voltage sweep.

As the peak area can be interpreted as an amount of charge ($Q=C\cdot V$), the difference in the peak areas in Figure 4.13 reflects the amount of charge trapped in deep traps. For the first voltage sweep, the trap density has been estimated by dividing the value of the peak area at 10 Hz ($0.22\cdot10^{-9}$ C) by the elementary charge and the volume of the organic layer in the diode ($7.7\cdot10^{-13}$ m^3). The resulting trap density is $1.8\cdot10^{21}$ m^{-3}, which is in good agreement with a trap density of 10^{22} m^{-3} estimated in the same way from EIS results [62]. In the same

way, for the second voltage sweep the trap density has been estimated to be $9.8 \cdot 10^{20}$ m^{-3}. So, approximately 45 % of the charges that are trapped during the first voltage sweep are still trapped during the second voltage sweep. The total trap density estimated from EIS measurements is smaller than the one derived from a *J-V* measurement in the previous paragraph (see Figure 4.9). This was expected as the value derived in the previous paragraph using TFL-SCLC theory is actually a bulk trap density. On the other hand, the traps monitored with EIS are located at the interface between PEDOT:PSS and PPV. As the exact dimensions of the interface layer are unknown, the trap density in this interface layer cannot be determined.

At room temperature, the deeply-trapped charge carriers are released after several hours (see Figure 4.14a). Detrapping of these charge carriers can be accelerated considerably by irradiation with UV light (see Figure 4.14 b).

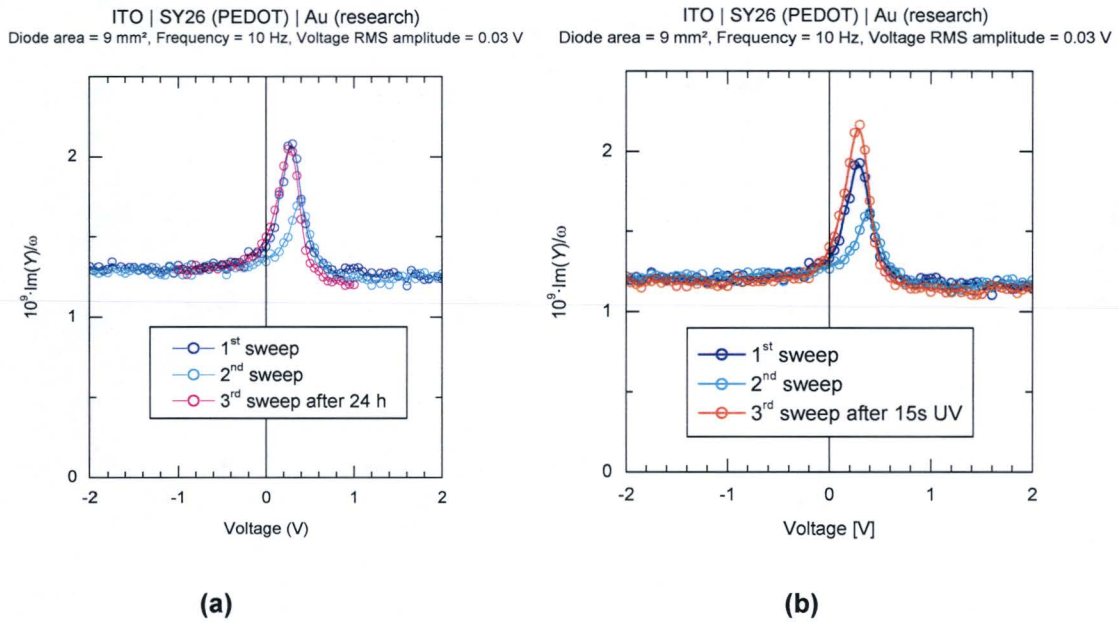

Figure 4.14 The capacitance of an ITO-SY-Au device expressed as the imaginary part of the admittance divided by the angular frequency plotted as a function of the applied bias voltage at a frequency of 10 Hz. The integration time was set at 5 s and V_m at 0.03 V. The diode area is 9 mm^2. (a) The third sweep (magenta colored) has been performed 24 hours after the second one. (b) The third sweep has been performed after a 15 s UV irradiation of the diode.

In the next paragraph EIS results concerning the reverse bias region (yellow colored in Figure 4.8) will be discussed.

4.3.3 The reverse bias region

If the reverse bias region of Figure 4.7 (which is redrawn in Figure 4.15) is examined closer, one can observe that the capacitance is independent of the applied voltage at each modulation frequency. Moreover, the measured capacitance is frequency-dependent. This behavior cannot be the result of a strong frequency-dependence of the relative dielectric constant of SY, because then it would also have led to an equally strong frequency-dependency in Figure 4.5. So, the absence of a strong frequency-dependence of the relative dielectric constant of SY (in Figure 4.5) suggests that the observed frequency-dependence of the capacitance in Figure 4.15 is a result of the presence of a PEDOT:PSS layer. Note, that this effect can also not result from the interaction of SY and PEDOT:PSS, or else it would have been visible in Figure 4.11 as well. Hence, one can correlate the shift of the voltage-independent capacitance at reverse bias to higher values as the modulation frequency decreases solely to the presence of a PEDOT:PSS layer.

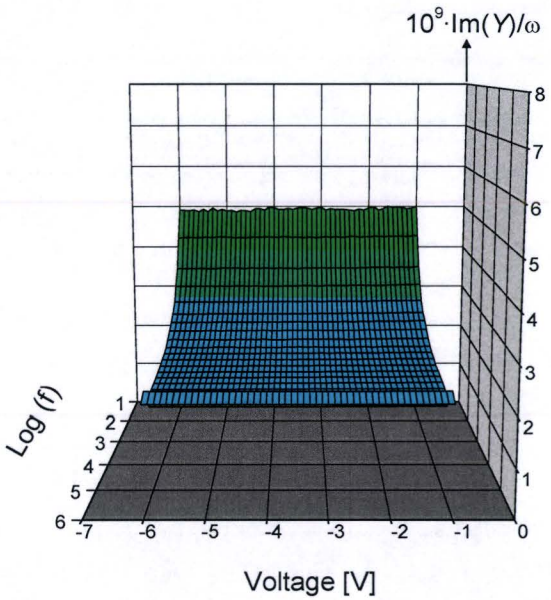

Figure 4.15 The reverse bias region of an ITO-PEDOT:PSS (150 nm)-SY (120 nm)-Au device. The PEDOT:PSS is the low-resistivity 5792/P2 (see Figure 4.7 for the complete bias range).

So, now we are convinced that the increase in capacitance in reverse bias is caused by the presence of a PEDOT:PSS layer, one might wonder which parameters influence this effect. Therefore several devices have been prepared with a SY layer (80 nm) on top of a PEDOT:PSS layer (150 nm) for which two kinds of PEDOT:PSS have been used: LVW 185 (high-resistivity) and LVW 186 (low-resistivity).

For both types of PEDOT:PSS also the Na^+ concentration has been varied, because it might be that these slow-moving ions could play a role in the increase of the capacitance at low frequency, if the modulation frequency is low enough for these ions to follow. The results for this series of experiments are given below.

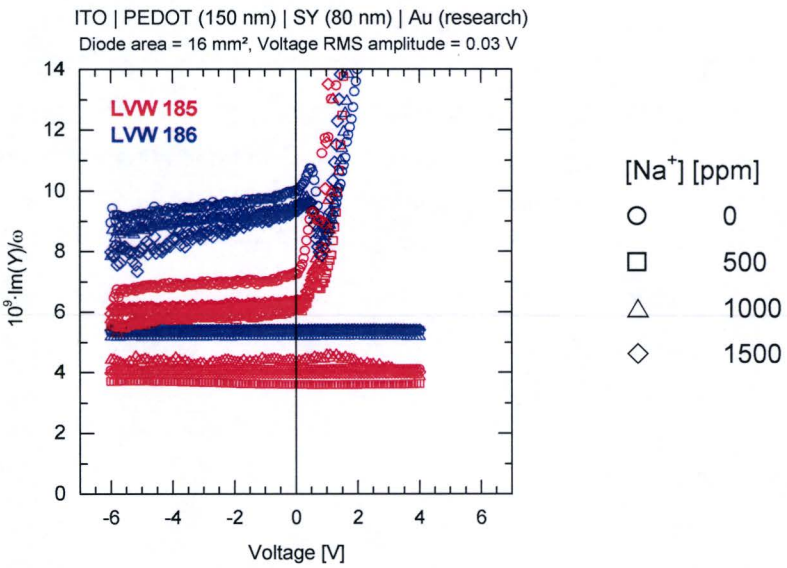

Figure 4.16 The capacitance of an ITO-PEDOT:PSS-SY-Au device expressed as the imaginary part of the admittance divided by the angular frequency plotted as a function of the applied bias voltage at a frequency of 10 Hz and 1 MHz. The PEDOT:PSS is either the high-resistivity LVW 185 (red) or the low-resistivity LVW 186 (blue). The various Na^+ concentrations are represented by different symbols as given in the legend. The integration time was set at 1 s and V_m at 0.03 V. The diode area is 16 mm^2.

Apparently, the Na^+ concentration does not have a significant influence on the reverse bias behavior. On the other hand, the resistivity of the PEDOT:PSS layer is an important parameter. For instance, the measured capacitance at 1 MHz is affected by the resistivity of the PEDOT:PSS layer. To get a clear picture of what is happening, the 0 ppm Na^+ concentration results of both types of PEDOT:PSS have been re-plotted again in Figure 4.17.

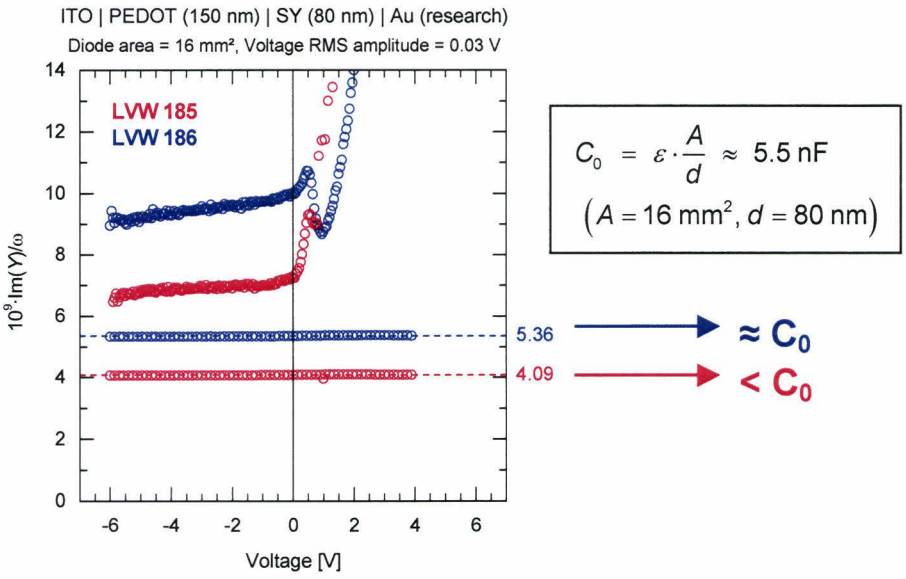

Figure 4.17 The capacitance of an ITO-PEDOT:PSS-SY-Au device expressed as the imaginary part of the admittance divided by the angular frequency plotted as a function of the applied bias voltage at a frequency of 10 Hz and 1 MHz. The PEDOT:PSS is either the high-resistivity LVW 185 (red) or the low-resistivity LVW 186 (blue). For both types of PEDOT:PSS, the Na^+ concentrations is 0 ppm. The integration time was set at 1 s and V_m at 0.03 V. The diode area is 16 mm^2.

For an 80 nm SY layer, the geometrical capacitance in a 16 mm^2 diode is about 5.5 nF (using a relative dielectric constant of 3.1). In Figure 4.17 one can observe that the capacitance of the diode containing the low-resistivity PEDOT:PSS has a value close to the geometrical capacitance of the SY layer, whereas the device containing the high-resistivity PEDOT:PSS has a significantly lower value.

At this point it is important to have a clear idea of how the device is built-up; therefore a cross-section of the device is shown in Figure 4.18.

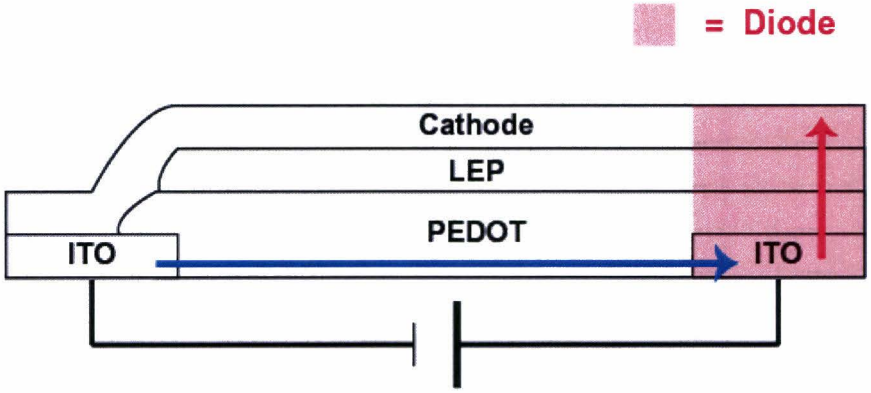

Figure 4.18 A schematic cross-section of a research device, in which the actual diode area is colored pink. The red arrow indicates the direction of the hole-current in forward bias via the vertical PEDOT:PSS area. The blue arrow indicates the direction of the ohmic hole-current observed in reverse bias via the lateral PEDOT:PSS area.

The red arrow in Figure 4.18 represents the SCL current that runs in forward bias through the diode, represented by the yellow colored region in Figure 4.19.

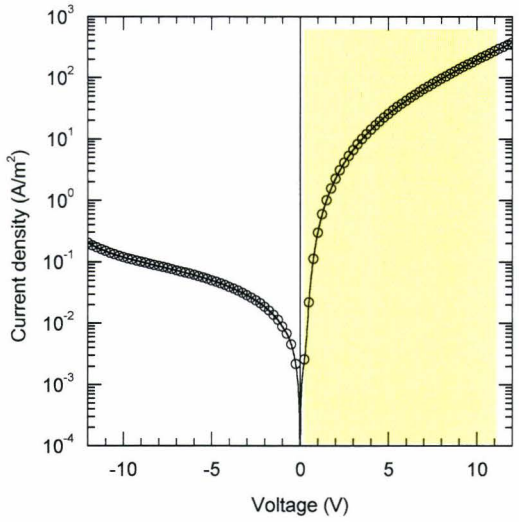

Figure 4.19 The current density plotted as a function of the applied voltage for an ITO-PEDOT:PSS (150 nm)-SY (80 nm)-Au device. The yellow area represents the flow of holes through the actual diode under forward bias.

The blue arrow in Figure 4.18 represents the lateral conductive path between the two ITO-structures via the PEDOT:PSS layer ($PEDOT_{//}$). The lateral current that flows through the PEDOT:PSS layer is usually termed "leakage current", which has an ohmic nature at low electric fields (at higher electric fields, the current through the PEDOT:PSS layer also starts to exhibit SCL features). Hence, the relation between current density and voltage would be $J \sim V$ instead of a power-law relation ($J \sim V^m$).

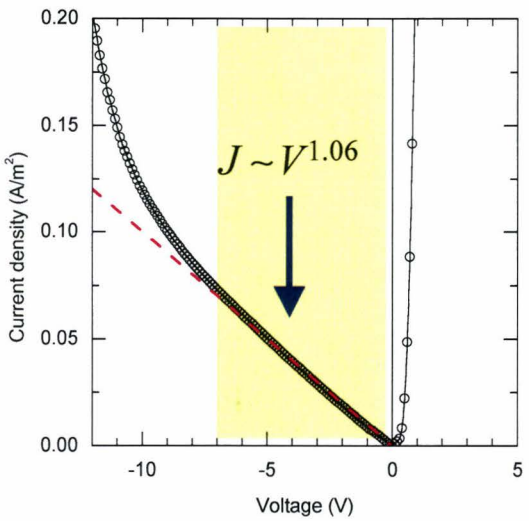

Figure 4.20 The current density plotted as a function of the applied voltage for an ITO-PEDOT:PSS (150 nm)-SY (80 nm)-Au device. The yellow area represents the lateral flow of holes through the PEDOT:PSS layer. A power-law fit yields a power of 1.06 for m in $J \sim V^m$.

A power-law fit in Figure 4.20 yields a power of 1.06, which indicates that the current density is linearly-dependent on the applied voltage (i.e. ohmic behavior). Another check has been applied to see that the current in reverse bias is really lateral conduction via the PEDOT:PSS layer. A linear fit applied to data obtained from a *I-V* measurement of a device with a layer of PEDOT:PSS (150 nm) of type 5792/P2 yielded a lateral resistivity of 160±10 Ωcm (see Figure 4.21), which is in good agreement with the value known for the lateral resistivity of PEDOT:PSS 5792/P2, which is 150 Ωcm [65].

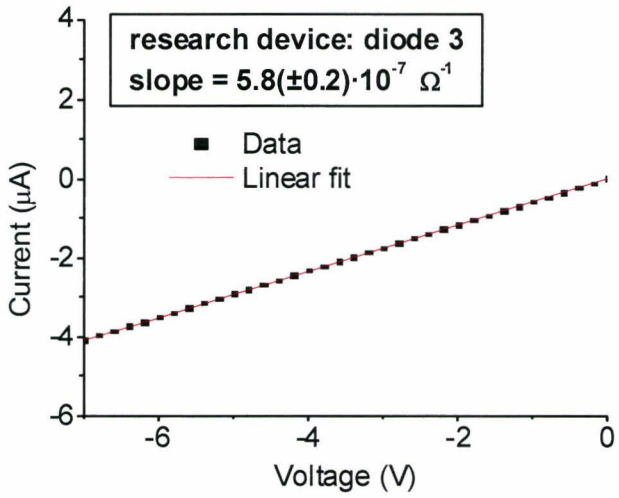

Figure 4.21 Current as a function of applied voltage an ITO-PEDOT:PSS (150 nm)-SY (80 nm)-Au device. The PEDOT:PSS is the low-resistivity PEDOT:PSS 5792/P2. The data are fitted to a linear relationship. As the lateral conduction would take place through an area of $9 \cdot 10^{-10}$ m^2 and over a distance of 1 mm, from the slope of the straight line a lateral resistivity of 160 Ωcm is calculated.

As mentioned before, the presence of a PEDOT:PSS layer is important for the impedance behavior at reverse bias. Therefore, it would be interesting to study the impedance of a device containing only a PEDOT:PSS layer. For this purpose the following research devices has been made: a PEDOT:PSS layer (150 nm) has been spin-coated on top of the ITO structures on the glass substrate. The pairs of ITO-structures (see Figure 3.2) have been contacted in order to measure the lateral PEDOT:PSS layer between them. The results of this experiment are shown below.

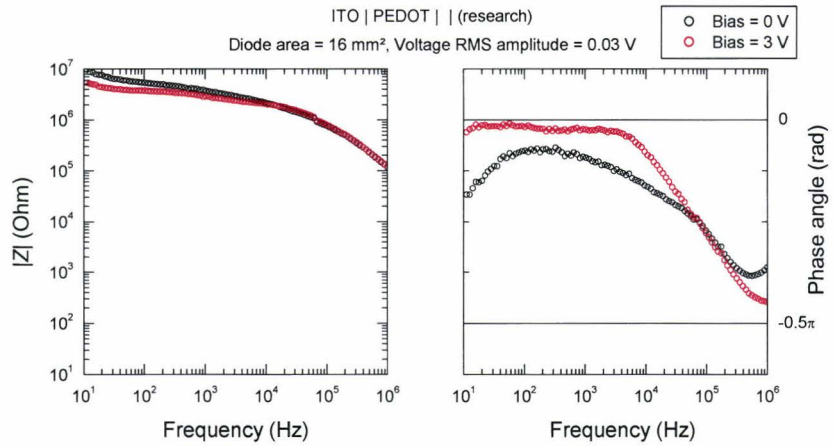

Figure 4.22 The Bode plot of the modulus of the impedance (|*Z*|) and the phase angle as a function of the modulation frequency at different background voltages (0 V and 3 V respectively). The integration time was set at 1 s, V_m=0.03 V. The diode area is 16 mm^2.

From Figure 4.22 it is clear that the device shows mainly resistive behavior, and only at high frequency capacitive behavior is observed. In conclusion, the PEDOT:PSS layer behaves as a capacitor at high frequency (1 MHz) and as a resistor at low frequency (10 Hz). However, due to geometrical reasons the capacitance of the lateral PEDOT:PSS region is very small compared to the capacitances of the layers in the actual diode, and can therefore be neglected. How to interpret this behavior in a working standard device?

Let us start by looking at the 1 MHz results of Figure 4.17 again and try to explain it by assuming that at this frequency the PEDOT:PSS layer can be described by a capacitor, i.e. both the lateral as the vertical PEDOT:PSS regions. So, the equivalent model of this diode at 1 MHz would be two capacitors C_0 and $C_{PEDOT\perp}$ connected in series, describing the actual diode containing an LEP layer on top of a PEDOT:PSS layer, which are on their turn connected in parallel with $C_{PEDOT||}$ (i.e. the capacitance of the lateral PEDOT:PSS area).

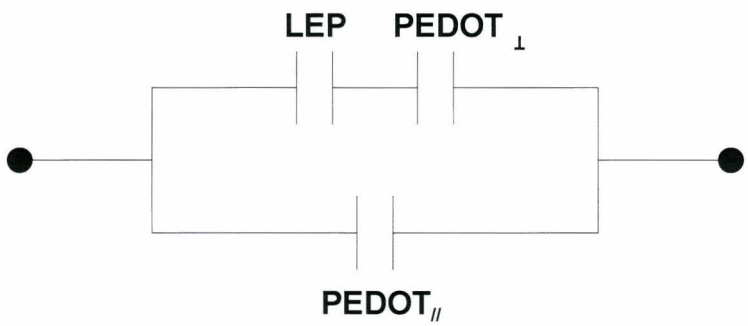

Figure 4.23 An equivalent circuit describing the impedance behavior at 1 MHz of a device containing an LEP layer on top of a PEDOT:PSS layer.

The expression for the total capacitance of this equivalent circuit is equal to:

$$C_{total} = C_{Diode} + C_{PEDOT||} \tag{4.1}$$

in which C_{Diode} is equal to

$$C_{Diode} = \frac{C_0 C_{PEDOT\perp}}{C_0 + C_{PEDOT\perp}} \tag{4.2}$$

As mentioned before, the capacitance of the "lateral leakage path" can be neglected compared to the capacitance of the diode and the capacitance that is effectively measured is that of the actual diode only. So, the expression for the total capacitance can be written as:

$$C_{total} = C_{Diode} = \frac{C_0}{\frac{C_0}{C_{PEDOT\perp}} + 1} \tag{4.3}$$

Generally, the lower the resistivity of the PEDOT:PSS is, the larger its relative dielectric constant will be. For a serial combination of two capacitances, if one of these capacitances is much smaller than the other, this capacitance will be effectively measured. This means that when a diode contains a layer of low-resistivity PEDOT:PSS, at high modulation frequency only the capacitance of the LEP layer is measured, which is evident from Figure 4.17. When the values of the two serially connected capacitances are comparable, an effective capacitance is measured that is lower than the capacitances of the two individual layers. This is what happens when a diode containing a layer of high-resistivity PEDOT:PSS is measured (see Figure 4.17).

The difference (i.e. shift) between the values at low (10 Hz) and high frequency (1 MHz) at reverse bias in Figure 4.17 is hypothesized to be the result of the resistive behavior of the lateral PEDOT:PSS area between the ITO-structures. When a potential is applied to the ITO anode of the diode, (a large part of) the PEDOT:PSS layer assumes the same potential. As a result, the anode is extended over the whole region between the two ITO-structures, hence inducing an equally large cathode area, *vide infra*.

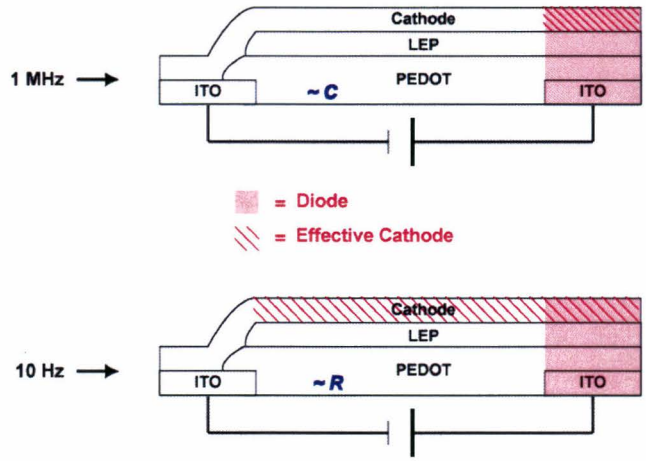

Figure 4.24 A schematic side-view of a research device, in which the hatched cathode area is larger at a frequency of 10 Hz than at a frequency of 1 MHz.

So, effectively the area of the diode is increased, which is now not confined to the red shaded area indicated in the upper part of Figure 4.24 but extends over the entire part of the LEP layer that is beneath the hatched cathode area indicated in the lower part of Figure 4.24. As a result the capacitance of the system increases.

By looking at the geometries and relative positions of the ITO structures comprising the two smallest diodes of a research device (see Figure 3.2) it is clear that at low frequency the capacitance at reverse bias can increase by a factor of about two at maximum.

This effect is not observed at high frequency, where the lateral PEDOT:PSS layer behaves more like a capacitor.

Another experiment has been performed in which devices with normal and reduced cathode areas have been measured with EIS in order to verify the above-mentioned hypothesis. The cathode area is reduced to approximately 50 % (see Figure 4.25). If the hypothesis is correct, this would yield approximately half of the value of the capacitance at low frequency (10 Hz).

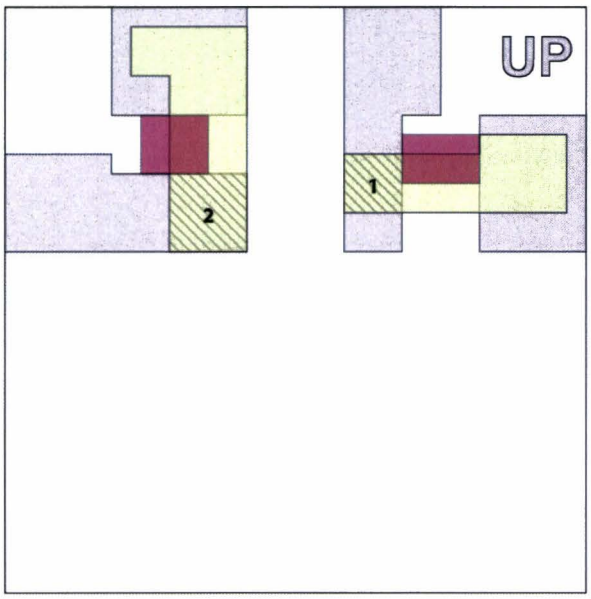

Figure 4.25 A schematic top view of the device substrates showing the ITO-structures (grey), and the cathode areas (yellow). For the diodes 1 and 2, the cathode area leading from the cathode contact area to the diode area (hatched) is reduced by a factor two by placing a piece of copper metal (red) in such a way that it blocks part of the mask opening.

The EIS results for the devices fabricated in a special way, as depicted in Figure 4.25, have been plotted together with the results obtained for research devices with the normal fabrication procedure in Figure 4.26.

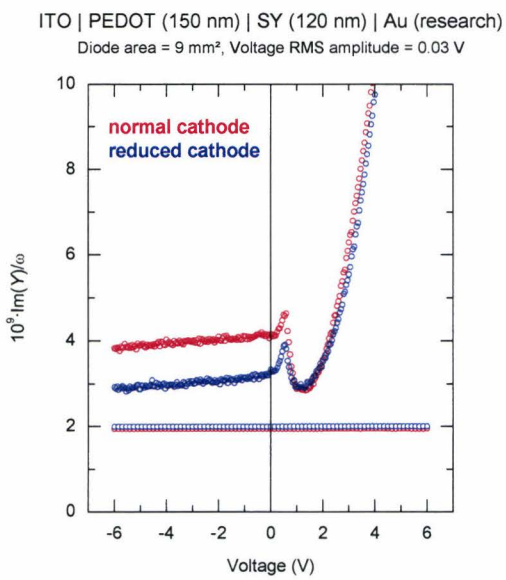

Figure 4.26 The capacitance of an ITO-PEDOT:PSS (150 nm)-SY (120 nm)-Au device expressed as the imaginary part of the admittance divided by the angular frequency plotted as a function of the applied bias voltage at a frequency of 10 Hz and 1 MHz. The data obtained on a normal device are shown in red, while the data obtained on a device with a reduced cathode area are shown in blue. The integration time was set at 1 s and V_m at 0.03 V. The diode area is 9 mm^2.

As one can see, the high-frequency (1 MHz) measurements are the same for both types of devices, so the cathode area does not affect the high-frequency (1 MHz) measurement. However, there is a distinct difference between the measurements at low frequency. The value of the voltage-independent capacitance at reverse bias is lower for the reduced cathode area than for the normal cathode area. The shift in the capacitance values for the reduced cathode device is approximately a factor two smaller than the shift for the normal cathode device. This is in agreement with a reduction of the cathode area by 50 %, thereby confirming the hypothesis concerning a frequency- dependent anode area $A(\omega)$. In this way, the expression for the frequency-dependent capacitance becomes:

$$C(\omega) = \varepsilon(\omega)\frac{A(\omega)}{d} \tag{4.4}$$

In the next section, devices containing other polymers than PPV such as poly(fluorene) (PFO) and poly(2,7-spirofluorene) (PSF) will be examined with EIS.

4.4 PFO and PSF as polymer and a PEDOT:PSS layer

PFO is a very pure material of high chemical order and low defect concentration and it has been reported that PFO shows an absence of trapping [59]. However, the behavior of PFO in the presence of a PEDOT:PSS layer could be different. This has been investigated by performing EIS on a device consisting of a PFO (80 nm) layer on top of a PEDOT:PSS layer (150 nm). The results of the EIS measurements are presented below.

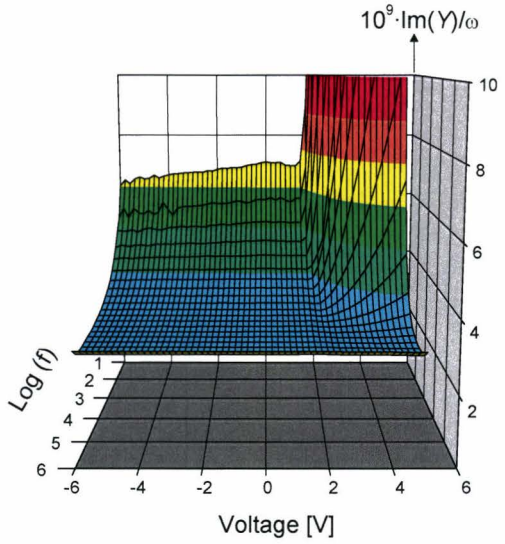

Figure 4.27 The capacitance of an ITO-PEDOT:PSS (150 nm)-PFO (80 nm)-Au device expressed as the imaginary part of the admittance divided by the angular frequency has been plotted as function of both the logarithm of the frequency as the applied bias voltage.

The plot of the EIS results for PFO looks very similar to that of PPV, except for the absence of the peak at V_{BI} in the case of PFO. Similarly as was observed in Figure 4.7, a voltage-independent capacitance is observed at reverse bias that increases as the modulation frequency decreases. Another resemblance between PPV and PFO is the increase in forward bias of the capacitance due to SCL current transport. However, this time the effect is much stronger for PFO.

The next polymer that has been examined with EIS is PSF. In addition to PFO, this polymer (PSF) has a repeat unit consisting of two fluorene units in staggered conformation (see Figure 1.3). The results of EIS performed on a device consisting of a PSF layer (80 nm) on top of a PEDOT:PSS layer (150 nm), is shown in Figure 4.28.

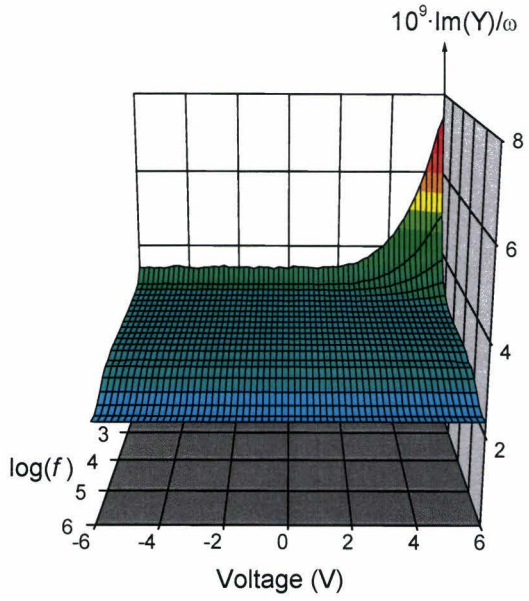

Figure 4.28 The capacitance of an ITO-PEDOT:PSS (150 nm)-PSF (80 nm)-Au device expressed as the imaginary part of the admittance divided by the angular frequency has been plotted as function of both the logarithm of the frequency as the applied bias voltage.

From Figure 4.28 it is clear that the PSF device behaves in a similar way as the PFO device although the magnitudes of the various effects are different.

What happens if one varies the thickness of the PEDOT:PSS layer? This has been done for both high-resistivity PEDOT:PSS and low-resistivity PEDOT:PSS in order to detect the influence of layer thickness variations in combination with the resistivity of PEDOT:PSS. For these experiments, bipolar devices were used that contained copolymers of fluorene and amines as LEP The EIS results for the low-resistivity PEDOT:PSS are shown below in Figure 4.29.

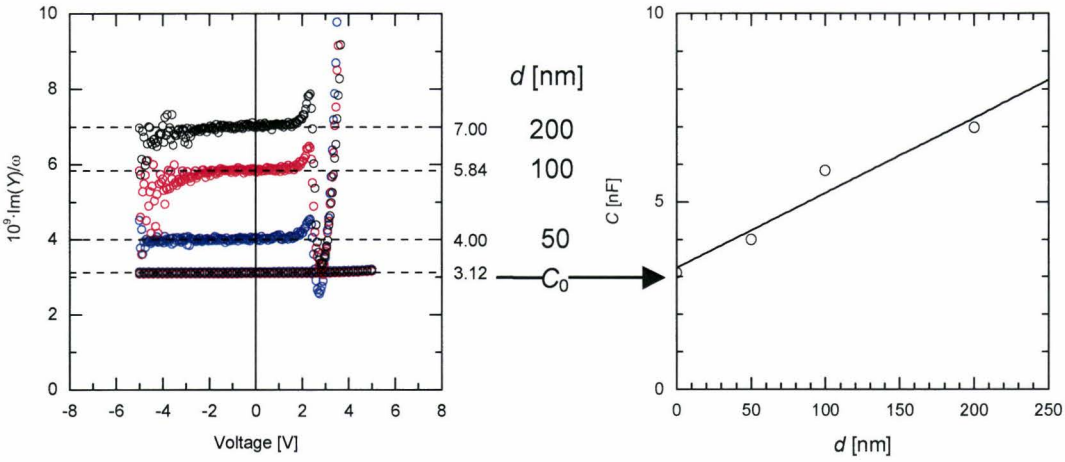

Figure 4.29 Left graph: the capacitance of ITO-PEDOT:PSS-LEP-Ba/Al devices expressed as the imaginary part of the admittance divided by the angular frequency plotted as a function of the applied bias voltage at frequencies of 10 Hz and 1 MHz. The PEDOT:PSS has a low resistivity and a varying layer thickness of 50 nm (blue), 100 nm (red), and 200 nm (black) respectively. Right graph: the value of the voltage-independent capacitance at reverse bias and low frequency plotted versus the PEDOT:PSS layer thickness. The solid line is a guide to the eye.

In Figure 4.29 one can see that at high frequency the geometrical capacitance of the LEP layer is measured while at low frequency the value of the voltage-independent capacitance under reverse bias increases with increasing PEDOT:PSS layer thickness. Judging from the graph on the right of Figure 4.29, this increase seems to be linear.

Previously, it was discussed that at high frequency only the actual diode is measured. When the diode contains low-resistivity PEDOT:PSS, only the capacitance of the LEP layer is effectively measured. This is also the case for the results shown in Figure 4.29, and explains why the high-frequency measurements all coincide.

The shift of the voltage-independent capacitance under reverse bias to higher values as the frequency decreases was ascribed to an increase of the effective diode area. On first sight, this does not imply a dependence on the thickness of the PEDOT:PSS layer. However, as the thickness of the PEDOT:PSS layer increases, the amount of charge that can be stored in this layer at a certain applied voltage increases and consequently the measured capacitance increases. The volume of the lateral PEDOT:PSS area increases linearly with the thickness of the PEDOT:PSS layer.

The EIS results for the high-resistivity PEDOT:PSS are shown below in Figure 4.30.

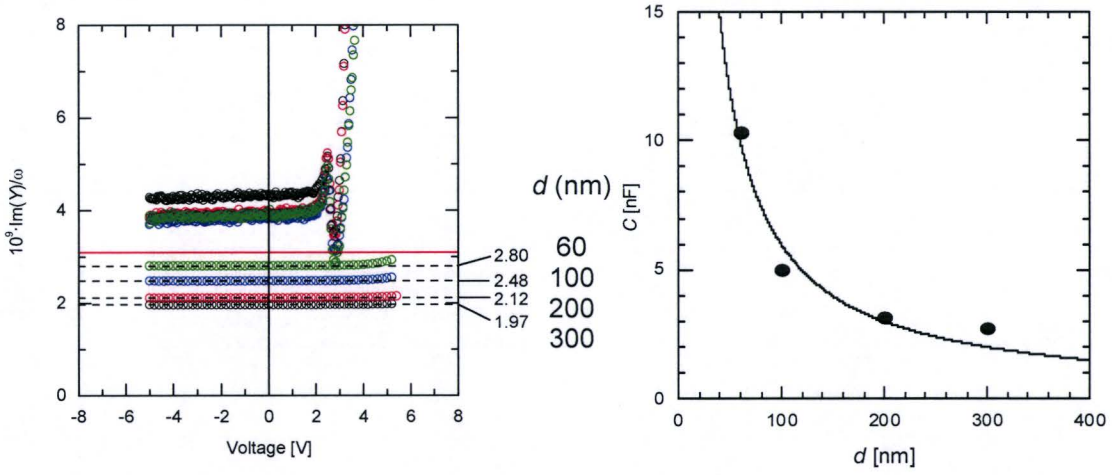

Figure 4.30 Left graph: the capacitance of ITO-PEDOT:PSS-LEP-Ba/Al devices expressed as the imaginary part of the admittance divided by the angular frequency plotted as a function of the applied bias voltage at a frequency 10 Hz and 1 MHz. The PEDOT:PSS has a high resistivity and a varying layer thickness of 60 nm, 100 nm, 200 nm, and 300 nm respectively. Right graph: the value of the voltage-independent capacitance at reverse bias and high frequency plotted versus the PEDOT:PSS thickness. The solid line (1/*d* dependence) is a guide to the eye.

For the high-resistivity PEDOT:PSS one can observe in Figure 4.30 that at low frequency the values of the capacitance in reverse bias are more or less independent of the PEDOT:PSS layer thickness. Conversely, the capacitance at high frequency is dependent on the PEDOT:PSS layer thickness: for thicker PEDOT:PSS layers, the measured capacitance decreases and judging from the right graph of Figure 4.30 this seems to follow a 1/*d* dependence.

At high frequency, only the actual diode is measured but in this case the capacitance of the PEDOT:PSS layer is comparable to that of the LEP layer and consequently an effective capacitance is measured that is lower than the capacitances of the two individual layers. Moreover, this effective capacitance should decrease according to a 1/*d* behavior as the PEDOT:PSS layer thickness increases.

The observations at low frequency are the result of the fact that the PEDOT:PSS has a high resistivity meaning that the charge carriers present in the PEDOT:PSS have a lower mobility. Consequently, the presence of these charge carriers becomes more apparent at frequencies lower than 10 Hz.

5 Conclusions

1. EIS results on a device containing a layer of an inert insulating polymer reveal a frequency- and voltage-independent capacitive behavior over a broad range of frequencies (10 Hz to 1 MHz) and applied voltages (−15 V to 15 V). The measured capacitance is equal to the geometrical capacitance.

2. The capacitance of a polymer light-emitting diode containing only a layer of a PPV derivative is frequency- and voltage-independent except at low frequency and an applied voltage above V_{BI}. Under these circumstances, the capacitance increases due to SCL current transport.

3. When a PEDOT:PSS layer is introduced in a polymer light-emitting diode containing a PPV derivative as LEP, three distinct areas can be observed in a low-frequency EIS measurement :
    - increase of the capacitance with increasing forward bias
    - capacitance peak at V_{BI}
    - voltage-independent capacitance at reverse bias

4. The increase of the capacitance with increasing forward bias is a result of the space charge limited nature of current transport.

5. The presence of the capacitance peak at V_{BI} is due to an interaction between PPV and PEDOT:PSS. This interaction results in the formation of traps at the PEDOT:PSS-PPV interface. At voltages close to V_{BI}, the traps are populated with charge carriers (holes) which results in the occurrence of a capacitance peak. The area of the peak is a measure of the amount of trapped charge. The first sweep captures the total amount of charge, whereas a second sweep captures only the shallow traps as the deeper traps have a relaxation time of several hours. Irradiation with UV accelerates the depopulation of the traps.

6. The voltage-independent capacitance at reverse bias increases with decreasing frequency when a PEDOT:PSS layer is present. This effect is due to the fact that the PEDOT:PSS layer assumes the same potential as the underlying ITO structure. At low frequencies, this results in an increase of the effective anode area, and a resulting increase of the measured capacitance. For the reverse bias behavior, the resistivity of the PEDOT:PSS layer is an important parameter, while the ion content does not influence this behavior.

7. Polymer light-emitting diodes containing PFO or PSF instead of PPV lack the presence of a capacitance peak at V_{BI}. This indicates that no interaction takes place between PEDOT:PSS and PFO or PSF that could lead to the formation of traps, as was the case when PPV is used instead. Although the exact nature of the chemical interaction between PEDOT:PSS and PPV remains unclear, the absence of such an interaction with PFO or PSF could indicate that somehow the vinylene bond of PPV is involved in the interaction with PEDOT:PSS.

8. When EIS measurements are performed on a polymer light-emitting diode at high modulation frequencies, only the actual diode is effectively measured. When the diode contains low-resistivity PEDOT:PSS, only the capacitance of the LEP layer is measured. When the diode contains high-resistivity PEDOT:PSS, an effective capacitance that is the series sum of the PEDOT:PSS layer capacitance and the LEP layer capacitance is measured.

6 Future work

One important goal is to build up a physical model for a polymer light-emitting diode, with which one can perform a quantitative analysis in order to predict in advance what certain device characteristics will be. The work presented in this report can be used as input for the development of such a device model.

To complete the qualitative understanding of the electrical impedance of polymer light-emitting diodes, measurements could be performed at frequencies lower than 10 Hz. For this purpose, the measurement setup as used for the research presented here has to be modified.

Furthermore, it would be interesting to study the exact nature of the charge traps that can be formed as a result of an interaction between PEDOT:PSS and the light-emitting polymer. To do this, a series of different polymers with slightly varying chemical compositions could be used.

7 Acknowledgements

First of all, I want to thank Professor Thijs Michels for the opportunity that he gave me for doing my master thesis at Philips Research (formerly known as Nat.Lab.) in Eindhoven. Also, I want to thank him for the faith that he has put in me. Special thanks I want to give to Professor Hans Hofstraat for allowing me to do my master thesis in his group (Polymers & Organic Chemistry) at Philips Research and for the kindness he has shown me. Another very kind person to whom I want to give my thanks is Professor Paul Blom. He gave us a warm welcome at the University of Groningen, where we had a very interesting discussion.

Next, I want to thank Peter Bobbert for the support and trust that he has put in me during my graduation. I have discovered underneath his extraordinary intelligence a warm and kind side that is always ready to help when it is needed. His disciplinary way of working together with his excellent interpersonal skills provided me enough guidance. It was a very pleasant and instructive experience to have him as a supervisor.

Then, I want to thank Addy van Dijken for all the guidance and support he showed towards me. Addy has teached me the basics of electrical impedance spectroscopy and of polymer light-emitting diodes in a very amusing and pleasant way. He is truly a great teacher and scientist due to a large amount of experience and knowledge. He has a very warm and kind-hearted character. It was a tremendous pleasure working with Addy.

Last but not least, I want to thank Alwin Marsman and Bianca van der Zande for the interesting discussions we had. Special thanks go to Dago de Leeuw, Klemens Brunner, Simone Vulto, Margreet de Kok, Michael Büchel, Eric Meulenkamp, Peter van de Weijer, Monique Vervest, Ton van den Biggelaar and Suzanne de Winter for their help. Also, I want to thank the students Mark, Florence, Sten, Stefan, Linda, Willy and Ruben for all the pleasant lunches we have had together full of laughter and joy.

8 Bibliography

1 H. C. F. Martens, Ph.D. Thesis, (Leiden University, 2000)

2 P. W. M. Blom and M. C. J. M. Vissenberg, Material Science and Engineering **27**, 53 (2000).

3 M. Pope, H. P. Kallman, and P. Magnante, J. Chem. Phys. **38**, 2042 (1963).

4 R. G. Kepler, Phys. Rev. **119**, 1226 (1960).

5 H. Mette and H. Pick, Z. Physik **134**, 566 (1953).

6 K. G. Kepler, Phys. Rev. **199**, 1226 (1960).

7 O. H. Le Blanc, J. Chem. Phys. **33**, 626 (1960).

8 K. C. Kao and W. Hwang, *Electrical Transport in Solids* (Pergamon, Oxford, 1981).

9 M. Pope and C. E. Swenberg, *Electronic Processes in Organic Crystals* (Clarendon Press, Oxford, 1982).

10 W. D. Gill, J. App. Phys. **43**, 5033 (1972).

11 D. M. Pai, J. Chem. Phys. **52**, 2285 (1970).

12 H. Hoegl., J. Phys. Chem. **69**, 755 (1965).

13 C. K. Chiang, C. R. Fincher, Y. W. Park, et al., Phys. Rev. Lett. **39**, 1098 (1977).

14 R. S. Kohlman, J. Joo, and A. J. Epstein, in *Physical Properties of Polymers Handbook*, edited by J. E. Mark (AIP Press, Woodburry, New York, 1996).

15 C. W. Tang and S. A. VanSlyke, Appl. Phys. Lett. **51**, 913 (1987).

16 H. Koezuka, A. Tsumara, and Y. Ando, Synth. Met. **18**, 699 (1987).

17 A. Tsumara, H. Koezuka, and Y. Ando, Synth. Met. **25**, 11 (1988).

18 F. Garnier, G. Horowitz, X. Z. Peng, et al., Adv. Mater. **2**, 592 (1990).

19 G. Horowitz, D. Fichou, X. Z. Peng, et al., Solid State Commun. **72**, 381 (1989).

20 J. H. Burroughes, D. D. C. Bradley, A. R. Brown, et al., Nature **347**, 539 (1990).

21 J.-W. van der Horst, Ph. D., (Eindhoven University of Technology, 2001)

22 J. McMurry, *Organic Chemistry* (Brooks/Cole Publishing Company: pacific Grove, California, 1988).

23 H. S. Woo, O. Lhost, S. C. Graham, et al., Synth. Met. **59**, 13 (1993).

24 Z. Shuai, J. L. Bredas, and W. P. Su, Chem. Phys. Lett. **228**, 301 (1994).

25 J. Cornil, D. Beljonne, Z. Shuai, et al., Chem. Phys. Lett. **247**, 425 (1995).

26 H. S. Nalwa, *Handbook of Advanced Electronic and Photonic Materials and Devices* (Academic Press, New York, 2001).

27 D. L. Gin, J. K. Avlynov, and A. G. MacDiarmid, Synth. Met. **66**, 169 (1994).

28 P. Kovacic and J. Oziomek, J. Org. Chem. **29**, 194 (1993).

29 M. Hamaguchi, H. Sawada, J. Kyokane, et al., Chem. Lett. **527** (1992).

30 D. M. Pai and B. E. Springett, Rev. Mod. Phys. **65**, 163 (1993).

31 A. J. Epstein and Y. Yang, in *Polymeric and Organic Electronic Materials: From Scientific Curisioty to Applications* (MRS bull. 22 (6), 1997).

32 N. S. Sariciftci, L. Smilowitz, A. J. Heeger, et al., Science **258**, 1474 (1992).

33 D. D. C. Bradley, A. R. Brown, P. L. Burn, et al., in *Solid State Sciences* (Springer, Heidelberg, 1992), Vol. 107, p. 304.

34 M. Alonso and E. J. Finn, *Fundamentele Natuurkunde Vol 4: Quantumfysica* (Delta Press, Overberg, 1994).

35 C. Möller and M. S. Plesset, Phys. Rev. **46**, 618 (1934).
36 A. Szabo and N. S. Ostlund, *Modern Quantum Chemistry: Introduction to Advanced Electronic Structure Theory* (McGraw-Hill, New York, 1989).
37 L. van Hove, Phys. Rev. **89**, 1189 (1953).
38 J. Veres, H. Becker, H. Sreitzer, et al., in *Electronic Transport in polyphenylene-vinylenes*, edited by W. Kreuder (Avecia&Covion, 2001).
39 V. Cleave, g. Yahioglu, P. Le Barny, et al., Adv. Mater. **11**, 285 (1999).
40 C. H. Chen and H. F. Meng, Phys. Rev. B **68**, 94112 (2003).
41 G. Burns, *Solid State Physics* (Academic Press, Boston, 1990).
42 A. Ruini, M. J. Caldas, G. Bussi, et al., Phys. Rev. Lett. **88**, 206403 (2002).
43 C. Adachi, M. A. Baldo, M. E. Thompson, et al., J. App. Phys. **90**, 5048 (2001).
44 F. Papadimitrakapoulos, K. Konstadinidis, T. M. Miller, et al., Chem. Mat. **6**, 1563 (1994).
45 A. R. Brown, D. D. C. Bradley, J. H. Burroughes, et al., Appl. Phys. Lett. **61**, 2793 (1992).
46 W. R. Salaneck and J. L. Bredas, Adv. Mater. **8**, 48 (1996).
47 P. W. M. Blom, M. J. M. de Jong, and J. J. M. Vleggaar, Appl. Phys. Lett. **68**, 3308 (1996).
48 I. D. Parker, J. App. Phys. **75**, 1656 (1994).
49 J. E. Mark and D. D. C. Bradley, Synth. Met. **57**, 4128 (1993).
50 M. A. Lampert and P. Mark, *Current Injection in Solids* (Academic Press, New York, 1970).
51 J. D. Jackson, *Classical Electrodynamics* (John Wiley & Sons, New York, 1998).
52 P. Langevin, Ann. Chem. Phys. **28**, 289 (1903).
53 D. R. Lide, in *Handbook of Chemistry and Physics* (CRC Press, Boca Raton, USA, 1992).
54 B. H. Cumpston, I. D. Parker, and K. F. Jensen, J. App. Phys. **81**, 3716 (1997).
55 J. R. MacDonald, *Impedance Spectroscopy: Emphasizing Solid Materials and Systems* (John Wiley & Sons, New York, 1987).
56 P. Mark and W. Helfrich, J. App. Phys. **33**, 205 (1962).
57 A. J. Campbell, D. D. C. Bradley, and D. G. Lidzey, J. App. Phys. **82**, 6326 (1997).
58 V. Kumar, S. C. Jain, A. K. Kapoor, et al., J. App. Phys. **94**, 1283 (2003).
59 F. Feller and D. Geschke, J. App. Phys. **93**, 2884 (2003).
60 C. Tanase, E. J. Meijer, P. W. M. Blom, et al., Phys. Rev. Lett. **91**, 216601 (2003).
61 A. van Dijken, A. Perro, E. A. Meulenkamp, et al., Organic Electronics **4**, 131 (2003).
62 I. H. Campbell and D. L. Smith, Appl. Phys. Lett. **66**, 3030 (1995).
63 M. Meier, S. Karg, and W. Riess, J. App. Phys. **82**, 1961 (1997).
64 I. N. Hulea, H. B. Brom, K. Brunner, et al., Synth. Met. **135-136**, 5 (2003).
65 M. Buchel, A. Habraken, H. van der Kruis, et al., *Nat.Lab. Technical Note 2002/025.*

9 Appendix A

Simplified Theory for trap-free insulator diode

The Maxwell equation [51] for the dielectric displacement $\vec{D}$ is given as

$$\vec{\nabla} \cdot \vec{D} = \rho_{free} \tag{A.1}$$

in which ρ_{free} is the free space charge density. The relation between the dielectric displacement $\vec{D}$ and the applied electric field $\vec{E}$ is

$$\vec{D} = \varepsilon_0 \vec{E} + \vec{P} = \varepsilon \vec{E} \tag{A.2}$$

in which $\vec{P}$ is the polarization field of the insulator used in the diode and ε_0 is the permittivity of vacuum and ε is the permittivity given by the following relation:

$$\varepsilon = \varepsilon_0 \kappa_E \tag{A.3}$$

where κ is the dielectric constant. The divergence of $\vec{P}$ is equal to the bound charge density ρ_{bound}:

$$-\vec{\nabla} \cdot \vec{P} = \rho_{bound} \tag{A.4}$$

The total charge density ρ is the sum of ρ_{free} and ρ_{bound}, and is equal to

$$\rho = ne \tag{A.5}$$

where n is the electron concentration and e is the electron charge. For a trap-free perfect insulator there is no bound charge density, so $\rho=\rho_{free}$ and therefore Equations (A.1), (A.2) and (A.5) combine to give the following Poisson equation

$$\frac{\varepsilon}{e} \vec{\nabla} \cdot \vec{E} = n \tag{A.6}$$

For the idealized case of a trap-free perfect insulator n is taken to be the spatially varying free electron concentration. So, the spatially varying trapped electron concentration as well as the constant thermal equilibrium electron concentration is taken to be zero for this idealized case [50]. The Maxwell equation for the effective magnetic field $\vec{H}$ inside the dielectric is given by

$$\vec{\nabla} \times \vec{H} = \frac{\partial \vec{D}}{\partial t} + \vec{J}_f \tag{A.7}$$

in which $\vec{J}_f$ is the free current density. The field $\vec{H}$ can be expressed in terms of the magnetic field $\vec{B}$ as

$$\vec{H} = \frac{\vec{B}}{\mu_0} - \vec{M} \tag{A.8}$$

in which μ_0 is the permeability of free space and $\vec{M}$ is the magnetization inside the dielectric. Equation (A.8) and Equation (A.2) are substituted into Maxwell Equation (A.7):

$$\vec{\nabla} \times \left(\frac{\vec{B}}{\mu_0} - \vec{M} \right) = \frac{\partial \varepsilon_0 \vec{E}}{t} + \frac{\partial \vec{P}}{\partial t} + \vec{J_f} \tag{A.9}$$

The total current density $\vec{J}$ is equal to the sum of the free current density $\vec{J}_f$, the magnetization current density $\vec{J}_M$ and the polarization current density $\vec{J}_P$:

$$\vec{J} = \vec{J}_f + \vec{J}_M + \vec{J}_P \tag{A.10}$$

where

$$\vec{J}_M = \vec{\nabla} \times \vec{M} \tag{A.11}$$

and

$$\vec{J}_P = \frac{\partial \vec{P}}{\partial t} \tag{A.12}$$

In the steady-state condition Equation (A.9) becomes:

$$\vec{\nabla} \times \vec{B} = \mu_0 \vec{J} \tag{A.13}$$

The divergence of Equation (A.13) leads by using the relation that the divergence of the rotation is zero to the following expression for $\vec{J}$:

$$\vec{\nabla} \cdot \vec{J} = 0 \tag{A.14}$$

This means that the total current density is constant. The total current density consists of the drift current density and the diffusion current density. The latter one is neglected because it is sizable only in the vicinity of the contacts, which on their turn are neglected because they are an infinite reservoir of electrons (or holes) available for injection. So, the total current density is equal to the drift current density:

$$\vec{J}_{drift} = \vec{v}_{drift} ne \tag{A.15}$$

where $\vec{v}_{drift}$ is the drift velocity of the electrons and is given by

$$\vec{v}_{drift} = \mu \vec{E} \tag{A.16}$$

This time μ is the mobility of the electrons (or holes) and from now on when the symbol μ is used the mobility is intended. So, the expression for $\vec{J}$ [1] becomes

$$\vec{J} = en\mu \vec{E} \tag{A.17}$$

If now equation (A.6) is substituted in Equation (A.17) by eliminating *n* it will result in

$$\vec{E}(\vec{\nabla} \cdot \vec{E}) = \frac{\vec{J}}{\varepsilon \mu} \tag{A.18}$$

If the cathode is situated at x=0 and the anode at x=L and the electric field and the current density are defined as pointing in the negative x-direction, then for a perfect trap-free insulator the following boundary condition can be applied: $\vec{E}(0)=0$. Using this boundary condition Equation (A.18) can be integrated to give

$$\vec{E}(x) = \sqrt{\frac{2\vec{J}}{\varepsilon \mu} x} \tag{A.19}$$

and

$$V(x) = \int_0^x \vec{E}(x')dx' = x\sqrt{\frac{8J}{9\varepsilon\mu}x} \tag{A.20}$$

By taking $x=L$ and $V=V(L)$ in the previous relation, the current-voltage characteristic is obtained:

$$J = \tfrac{9}{8}\varepsilon\mu\frac{V^2}{L^3} \tag{A.21}$$

Equation (A.21) is also called the trap-free square law or the Mott-Gurney square law. From electrostatics the following expression is known for the total charge Q:

$$Q = CV \tag{A.22}$$

For a trap-free perfect insulator all injected electrons remain free, i.e. in the conduction band, and contribute to the space charge. The total charge may be written then also like

$$Q = JAt \tag{A.23}$$

where A is the area of the diode and t is the transit time for a free electron between cathode and anode, or in other words the interelectrode transit time, and is given by

$$t = \tfrac{4}{3}\frac{L^2}{\mu V} \tag{A.24}$$

When Equation (A.24), (A.23) and (A.21) are substituted into Equation (A.22), then one can find the following expression for the capacitance C

$$C = \tfrac{9}{8}\tfrac{4}{3}\frac{\varepsilon A}{L} \tag{A.25}$$

The geometrical capacitance C_0 is given by

$$C_0 = \frac{\varepsilon A}{L} \tag{A.26}$$

So, when a steady-state one-carrier SCL current flows, the capacitance of a trap-free perfect insulator is equal to:

$$C = \tfrac{3}{2}C_0 \tag{A.27}$$

10 Appendix B

Trap-filled limit space-charge limited current

In polymer light-emitting diodes where the current density (J) and the applied bias voltage (V) no longer have a power law dependency according to standard space-charge limited current (SCLC) theory, a new model has to be used. This model is the trap-filled limit SCLC (TFL-SCLC) [50], which assumes in addition to standard SCLC an exponential distribution of traps characterized by two parameters: the density of traps (N_t) and the constant of distribution E_t. This characteristic energy is often expressed as a characteristic temperature T_C

$$E_t = kT_C \tag{B.1}$$

in which k is the Boltzmann constant. The characteristic temperature is determined from the power law exponent

$$l = \frac{T_C}{T} \tag{B.2}$$

in which T is the measurement temperature. The power-law between J and V is then given by the following relationship [58]

$$J = K \cdot V^{l+1} \tag{B.3}$$

In which K is equal to

$$K = e^{l-1}\mu N_V \left(\frac{2l+1}{l+1}\right)^{l+1} \left(\frac{l}{l+1}\frac{\kappa\varepsilon_0}{N_t}\right)^{l} \frac{1}{d^{2l+1}} \tag{B.4}$$

Here, ε_0 is the permittivity of free space, κ is the relative dielectric constant of the polymer, μ is the hole-mobility, N_V is the density of states in the valence band, e is the elementary charge and d is the thickness of the sample. The logarithm of both sides of Equation B.3 yields the following expression

$$\log(J) = \log(K) + (l+1)\log(V) \tag{B.5}$$

When the logarithm of J is plotted as a function of the logarithm of V, then one can use this expression in a fit to obtain various parameters such as E_t and N_t.